Received: 11 April 2023 | Revised: 10 November 2023 | Accepted: 14 November 2023

DOI: 10.1002/jrs.6628

REVIEW ARTICLE

Journal of RAMAN SPECTROSCOPY WILEY

Waveguide-based Raman enhancement strategies

Junyi Zhao[1,2] | Xiumian Cao[1,3] | Weiqing Xu[1,2] | Shuping Xu[1,2,4,5]

[1]State Key Laboratory of Supramolecular Structure and Materials, College of Chemistry, Jilin University, Changchun, China

[2]Institute of Theoretical Chemistry, College of Chemistry, Jilin University, Changchun, China

[3]College of Physics, Jilin University, Changchun, China

[4]State Key Laboratory of Applied Optics, Changchun Institute of Optics, Fine Mechanics and Physics, Chinese Academy of Sciences, Changchun, China

[5]Center for Supramolecular Chemical Biology, College of Chemistry, Jilin University, Changchun, China

Correspondence
Shuping Xu, State Key Laboratory of Supramolecular Structure and Materials, College of Chemistry, Jilin University, Changchun 130012, China.
Email: xusp@jlu.edu.cn

Funding information
National Natural Science Foundation of China, Grant/Award Numbers: 22173035, 21873039, 21827805; Fundamental Research Funds for the Central Universities, Science and Technology Development Program Projects of Jilin Province, Grant/Award Number: 20220101046JC; Opening Project of the State Key Laboratory of Applied Optics, Grant/Award Number: SKLAO2021001A14; Interdisciplinary Integration Innovation Project of Jilin University, Grant/Award Number: JLUXKJC2020106

Abstract

Waveguide-enhanced Raman scattering (WERS) is a powerful branch of enhanced Raman technologies that has gained significant progress in recent years because of its advantages, such as reproducibility and robustness. As a complementary tool to surface-enhanced Raman spectroscopy (SERS), WERS provides a powerful solution for reproducible quantification of analytes. According to different Raman enhancement mechanisms, five major WERS implementation strategies, namely, (1) single-mode dielectric waveguide, (2) liquid core waveguide, (3) metal cladding waveguide, (4) resonance mirror waveguide, and (5) double metal cladding waveguide, are classified and described in detail in this review. The flexibility of WERS structures makes them easy to be integrated with 2D devices to obtain a complete on-chip detection scheme, allowing the WERS chip to combine excitation, detection, and data analysis in integrated chips, providing a powerful prospect for real-time and on-site analysis of target samples. This article highlights the principles, implementations, and application scenarios of WERS techniques and evaluates their advantages and limitations, respectively. Finally, the strengths and weaknesses of WERS techniques are summarized, and promising future applications are proposed. This review provides a panoramic view for researchers interested in waveguide-enhanced Raman technology.

KEYWORDS

integrated photonics, Raman spectroscopy, SERS, waveguide, waveguide-enhanced Raman scattering

1 | INTRODUCTION

With the continuous pursuit of people's quality of life, the demand for rapid, nondestructive, and real-time detection of target analytes is also increasing in food safety, environmental monitoring, medical health, and other fields. The development of optical sensors offers numerous solutions in these fields. A series of qualitative and quantitative analysis methods have been developed, such as colorimetry,[1,2] fluorescence,[3,4] and refractive

index methods.[5,6] These methods are highly sensitive to molecular bonding events and suitable for dynamic measurements. Nevertheless, they provide less information at the chemical and molecular levels, and nonspecific adsorption interference may bring problems in multicomplex sensing systems, which may lead to a misunderstanding of the original chemical process.

Raman scattering can obtain molecular fingerprint information, which is conducive to understanding the chemical bonds and conformational changes of molecules with no need for external labels. Raman spectra allow visible to near-infrared light to excite, and its spectral profile reflects the frequency shift of the Stokes light relative to the incident wavelength. Water's Raman signals are mainly distributed in high wavenumbers away from many organic matters (usually below 2000 cm^{-1}). Thus, Raman spectroscopy is available for detecting samples in aqueous systems. One well-known drawback is that the Raman effect is too weak because the Raman scattering cross-section of analytes is only $\sim 10^{-31}$–10^{-29} cm^2 per molecule,[7] which significantly limits its applications in analytical fields.

In order to amplify weak Raman spectroscopic signals, Raman enhancement technology has received extensive attention. The most famous branch is surface-enhanced Raman scattering (SERS), which is an extraordinary spectral enhancement phenomenon dependent on SERS substrates. SERS was first reported in 1974 by observing the enhanced Raman signals of pyridine on a rough silver electrode surface.[8] In recent years, many excellent reviews have systematically summarized its progress in different aspects.[9–14] SERS allows the detection of trace analytes on metal surfaces, even arriving at the single-molecule level.[15,16] Compared with fluorescence spectroscopy, SERS spectroscopy is resistant to photobleaching and photodegradation compared with fluorescence emission and suitable for high-power and long-term detections. It also enables multiplex detection under one excitation wavelength. Various plasmonic and semiconductor SERS substrates are alternatives.[17] These advantages make SERS available for chemical reaction monitoring,[11] bioanalysis,[14] medical,[13] and spectral imaging.[18] Besides the widespread SERS, low signal reproducibility caused by the poor repeatability and the uncontrollable substrate surface robustness is still a severe problem bothering SERS studies. In order to overcome this problem, dielectric-enhanced Raman spectroscopy, which benefits from highly ordered and stable substrates, has flourished in recent years.[19] As one of the important branches, waveguide-enhanced Raman scattering (WERS) has received increasingly widespread attention. Unlike other SERS strategies relying on metallic structures, the unique and outstanding light-regulation ability of dielectric structures at the nanoscale makes WERS more controllable and reproducible, which makes WERS promising in interfacial SERS detections.

The enhancement mechanisms of Raman signal in WERS can be broadly classified into wide-area enhancement based on large interaction volume and confined-area enhancement based on a strong electromagnetic field in relatively small action volume. The former mainly realizes the overall signal amplification by collecting the cumulative scattering signals of molecules on the whole light guide path, whereas the latter is similar to SERS, which mainly enhances the Raman signal by increasing the local electromagnetic field intensity. Depending on how the electromagnetic field interacts with analytes, two excitation ways in WERS can be found: ① evanescent field excitation and ② direct excitation by light propagated within a waveguide structure. Based on the waveguide structures and enhancement mechanisms, WERS can be divided into five categories (Figure 1): (1) single-mode dielectric waveguide excited by a long-range evanescent field, (2) liquid core waveguide (LCW) directly excited by the long-range waveguide light, (3) metal cladding waveguide (MCW), (4) resonant mirror waveguide excited by a confined-range evanescent field, and (5) double-layer MCW directly excited by the confined-range guiding light. WERS can solve many existing problems of SERS to some extent and provide many unique advantages over SERS.[20] For instance, compared with the complex plasmonic substrates, the waveguide substrate is simple and robust, with high stability and signal repeatability. Waveguide structures allow wide-band excitation. The electric field component on the plasmonic surface is usually parallel to the normal direction, whereas the waveguide structure permits independent detections of two orthogonal polarizations.

In this review, starting from the various excitation modes mentioned above, we will give an overview of the theoretical mechanisms and applications of five-typed WERS geometries, as shown in Figure 1. In the process of enumerating excellent investigations, we will discuss the advantages and limitations of different enhancement strategies and summarize the opportunities and challenges of WERS.

2 | WERS STRUCTURE BASED ON LONG-RANGE ENHANCEMENT

Optical waveguides are one of the most basic photonic elements for guiding waves along specific structures. They are usually composed of transparent media with a

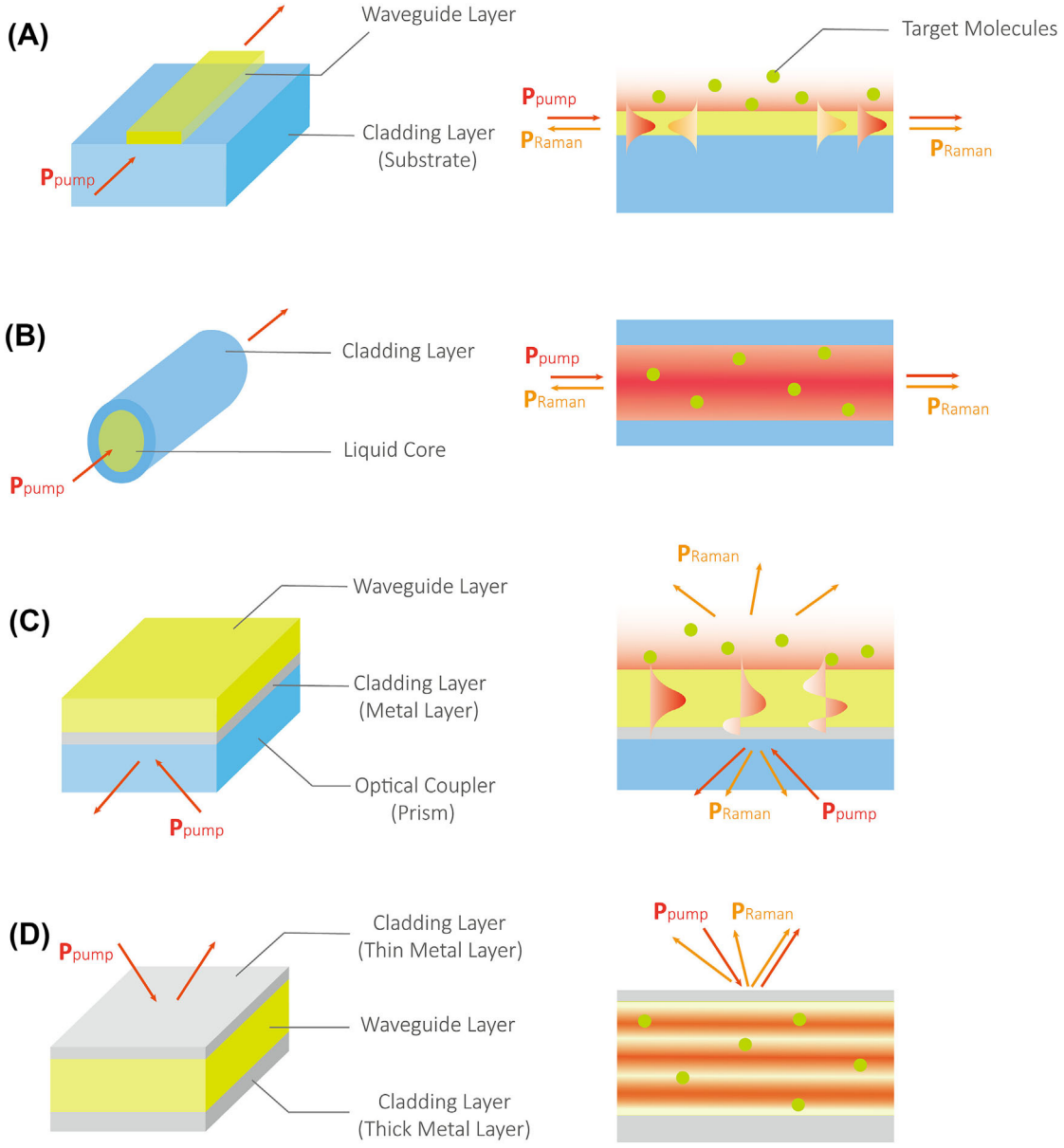

FIGURE 1 Schematic diagram of the structure, excitation, and collection methods of four typical waveguide-enhanced Raman scattering substrates. (A) Single-mode dielectric waveguide excited by a long-range evanescent field. (B) Liquid core waveguide directly excited by the long-range waveguide light. (C) Metal cladding waveguide excited by a confined-range evanescent field. The overall structure of the RCW is similar to that of the MCW, except that in the former case, the metal layer is replaced by a micron-thick dielectric layer. (D) Double-layer metal cladding waveguide directly excited by the confined-range guide light.

higher refractive index than their surroundings. The light ray propagating in the waveguide is restricted in the guiding layer via total internal reflection (TIR). Long-range enhancement-based WERS achieves the cumulative amplification of Raman signals by increasing the volume of light interacting with molecules. In this section, single-mode dielectric waveguides and LCWs, both of which achieve long-range excitation, are introduced systematically. One difference between both is that the evanescent field on the waveguide surface interacts with the molecules in the single-mode dielectric waveguide, whereas in the LCW, the liquid with target molecules serves as the waveguide layer. Single-mode dielectric waveguides can be divided into ① slab dielectric waveguides, ② strip dielectric waveguides, and ③ slot dielectric waveguides according to the core geometry. Depending on differences in cladding designs, LCWs can be cataloged as ① capillary LCWs, ② photonic crystal fiber LCWs, ③ liquid cladding LCWs, ④ anti-resonant LCWs, and ⑤ optical jet LCWs. Each waveguide structure corresponds to its own application scenario, and we will also analyze their respective advantages and limitations.

2.1 | Single-mode dielectric waveguide

The dielectric waveguide is composed of trilayers, including a substrate, a cladding layer, and a core layer (waveguide layer), as shown in Figure 2A. When the refractive index of the waveguide layer is higher than that of the cladding and substrate, multiple TIRs of the light can occur in the waveguide layer. When the thickness and refractive index of the waveguide layer meet certain matching conditions, the light will resonate (called mode), and the incident electric field will be amplified in the dielectric layer and propagate forward along the waveguide layer. The waveguide can support a limited number of transverse electric (TE) and transverse magnetic (TM) modes, both of which have a corresponding cut-off thickness under different modes. When a beam is coupled into a multimode waveguide, rays with different incident angles give rise to various modes, and how many modes are decided by the wavelength of the light, the waveguide geometric structures, and their relative refractive indices. When all other modes except the fundamental mode have been cut off with certain conditions, this waveguide is called a single-mode waveguide. The most direct way to achieve a single mode is to compress the size of the waveguide layer so that it cannot meet the cut-off thickness of the high-order modes (the details will be introduced below). The electric field of the guided mode is not entirely confined to the waveguide layer but penetrates the cladding and substrate and decays from the surface, which is called the evanescent field. The evanescent field can excite the Raman signal of adsorbed molecules near the waveguide surface, as shown in Figure 1A.

2.1.1 | Principles and evaluation methods

The theory of WERS was described in the early work of Kanger et al.[24] The intensity of Raman signal is proportional to the electric field intensity of the evanescent field related to the refractive index and the thickness of the waveguide layer. Increasing the refractive index of the waveguide layer leads to a corresponding compression of the cutoff thickness, which in turn leads to a reduction of the optimal working thickness of the

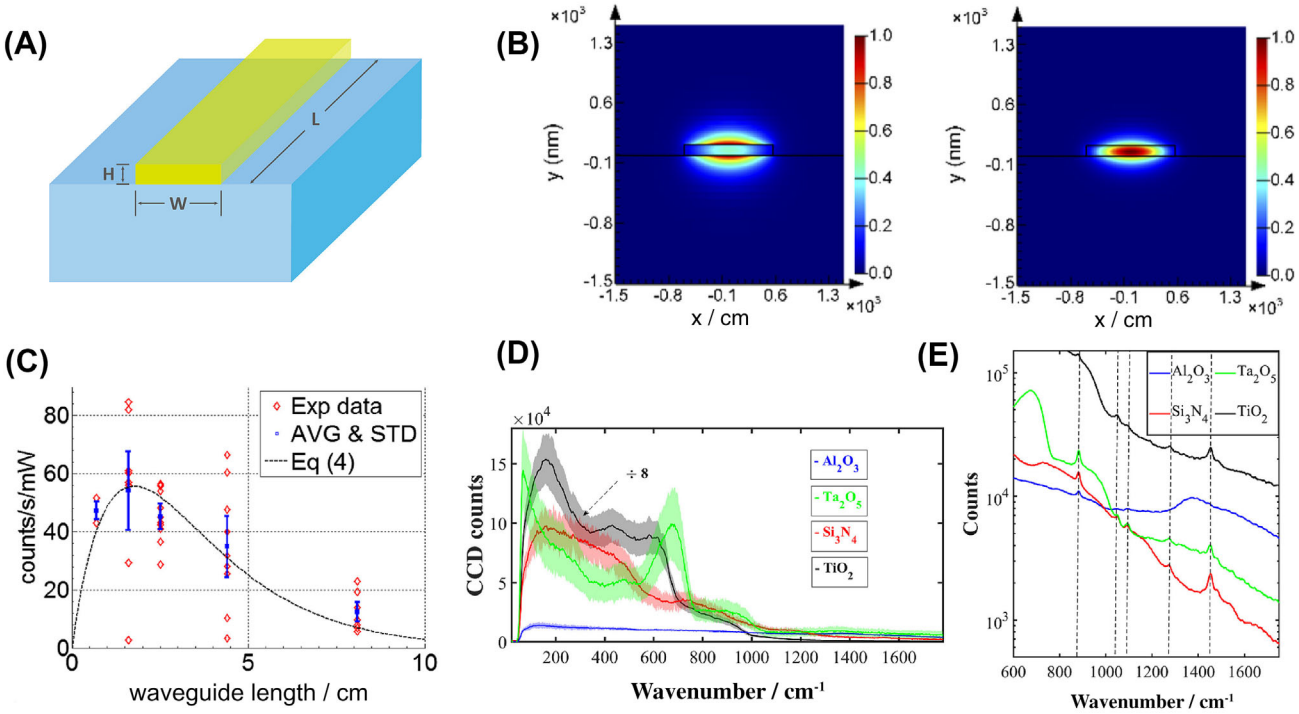

FIGURE 2 (A) Structure of a typical single-mode strip dielectric waveguide. (B) Diagram of TM (left) and TM (right) mode distribution of Si_3N_4 strip dielectric waveguide platform, simulated with toluene as the upper cladding. Reproduced with permission.[21] Copyright 2020, The Optical Society. (C) The Raman collection efficiency of 819-cm^{-1} peak of isopropanol molecules on a Si_3N_4 strip dielectric waveguide excited by different wavelengths. Red diamond markers: actual measured data. Blue solid square with error bars: mean and standard deviation. Black dashed line: theoretical fit to respective equations as a guide for the eye. Reproduced with permission.[22] Copyright 2014, The Optical Society. (D) Background scattering from four different waveguide platforms normalized by length factor and coupling efficiency. (E) The Raman spectra of ethanol as the upper cladding are obtained. The dotted lines represent the 880-, 1054-, 1098-, 1275-, and 1456-cm^{-1} Raman modes of ethanol. (D) and (E) were reprinted with permission.[23] Copyright 2019, The Optical Society.

waveguide layer. For example, when ZnO with a refractive index of 2.0 was employed as the core layer in a single-mode waveguide, the thickness of the core layer can be optimized to be 100–150 nm under the irradiation of 514.5-nm pump light to obtain the maximum of the evanescent field intensity at the waveguide surface.[24]

A systematic WERS theory was given by Dhakal et al.,[22,25] and many review articles also summarized the relevant theories.[20,26] Here, a conclusive expression will be given, and more detailed derivation processes can refer to the relevant literature mentioned above.

Assuming that a pump light with a power of P_{in} irradiates the input surface of a single-mode waveguide, propagates along the waveguide, and excites the molecules on the waveguide surface, the spontaneous Raman scattering of the molecules is coupled to the end side of the waveguide through the waveguide structure and collected by an objective lens. Half of the scattering signals coupled into the waveguide propagate forward, and half propagate backward. When analytes uniformly adsorb the waveguide layers with a density of ρ, their Raman scattering propagates forward and is collected at the waveguide end face on the opposite side of the pump light. The ratio of the signal power P_{col} collected at the end toward the power P_{in} of the pump light can be expressed as (1)[20,25]:

$$\frac{P_{col}(L)}{P_{in}} = \frac{1}{2}\rho\sigma\eta_0\gamma_{in}\gamma_{out}e^{-a_pL}L \tag{1}$$

γ_{in} is the coupling efficiency of the pump light to the waveguide, γ_{out} is the output efficiency of the signal, L is the length of the waveguide structure, and η_0 represents the specific conversion efficiency of the waveguide, which is an important parameter to evaluate the enhancement performance of a waveguide. σ is the Raman scattering cross-section. a_p is the loss of the pump light in the waveguide, and it is assumed that a_p is the same as the Stokes light in the waveguide. The coefficient 1/2 indicates that only one side of the waveguide is collected. The length of the waveguide decides the acquisition efficiency of the Raman scattering signal. Owing to the transmission light loss in the waveguide, there exists an optimal waveguide length $L = 1/a_p$ for the maximum signal acquisition efficiency. The optimal waveguide length was also confirmed in experiments by measuring the Raman signal of the isopropanol, as shown in Figure 2C.[22] As for a single-mode waveguide, a waveguide length shorter than the pump wavelength by 20 times can provide an efficiency equivalent to the confocal microscope. If the typical 1 dB/cm single-mode waveguide loss is considered, there will be no significant losses on the pump and scattering signals, even if the waveguide length exceeds 1 cm.[26]

It should be noted that the models for the WERS theory are all based on the single-mode waveguide, because the beam divergence angle collected at the end side of the single-mode waveguide is the smallest,[26] which allows the collection efficiency to increase as much as possible and the loss goes to the lowest when the numerical aperture of the collection device is given. The pump light that excites the electric dipole on the surface of the waveguide enters the waveguide by means of prism coupling,[27] grating coupling,[28] end side irradiation,[25] and propagates forward, respectively. The collection of Raman scattering can be from (1) the free space on the surface or (2) the end side of the waveguide, in which the end side collection is classified into two types, front-end collection, and back-end collection. Equation (1) describes that the pump light coupled into the waveguide excites the target molecules and the pump and Stokes light were collected from the waveguide end. This method gives a much higher collection efficiency than the collection way using an objective lens collection in free space,[29,30] whereas it is more conducive to the integration with compact spectroscopic instruments. Objective excitation and acquisition at the end-side of the waveguide is the most commonly used configuration in reported WERS setups.

In the case of the backward propagating Raman signal, a ratio of P_{col} to P_{in} is given by the following Formula (2)[20,23]:

$$\frac{P_{col}(L)}{P_{in}} = \frac{1}{2}\rho\sigma\eta_0\gamma_{in}\gamma_{out}\frac{1-e^{-2a_pL}}{2a_p} \tag{2}$$

In the backward collection, the overall signal collection efficiency as a function of waveguide length rises monotonically, although the light transmission loss remains. This enables the waveguide length to be adjustable flexibly according to the actual needs.

For the commonly used coupling strategies from the light to a waveguide, focusing the pump light through the objective lens and directly irradiating it on the end side are frequently adopted. However, this scheme needs cumbersome operations, such as aligning and stabilizing optical paths. Utilizing a grating to couple a pump light is a feasible way to simplify the light path.[28] Owing to many optimized structural parameters, the coupling efficiency will also be improved, and the energy loss will be weakened relative to the objective lens excitation.

2.1.2 | Slab dielectric waveguide

WERS has been proven to be a powerful technique for studying thin film molecules for decades. The slab (planar) waveguide is the simplest waveguide structure used in WERS. The pump light is coupled into the waveguide through a prism or the end section of a waveguide, and then it can propagate several centimeters along the waveguide layer to excite the Raman scattering of the thin film molecular layer adjacent to the waveguide. The Raman scattering signals accumulated along the waveguide are collected through the objective lens in free space or the end section of the waveguide. In 1974, Levy et al. reported the Raman spectra of methyl methacrylate films, which also played as the waveguide guiding layer with several microns.[31] This study proves that this configuration is available for thin film molecules from hundreds of nanometers to several microns. However, a waveguide mode is unimplemented if the molecular layer thickness is less than 100 nm. Then, on this basis, Rabolt et al. obtained the Raman spectra of an 80-nm polystyrene thin film by placing a low refractive index film as a cladding layer above a high refractive index waveguide layer.[32] Walker et al. measured the resonance Raman spectrum of cytochrome c (Cytc) excited at 514.5 nm on a silicon waveguide with a refractive index of 1.52.[33] A stronger evanescent field can lead to stronger Raman scattering signals, and the surface evanescent field intensity can be effectively modulated by changing the refractive index and the thickness of the waveguide layer. Kanger et al.[24] constructed a ZnO waveguide with a high refractive index ($n = 2.0$) and a low thickness (about 110–130 nm) to obtain the non-resonance Raman spectra of dimyristoyl phosphatidylethanolamine (DMPE) lipid monolayer and bovine serum albumin monolayer on the waveguide surface with a high signal-to-noise ratio (SNR). Next, they applied this ZnO thin film waveguide in the polarized Raman spectra of Cytc and nickel-octaethyl porphyrin (NiOEP) on the surface,[34] to establish a relationship between the Pullman depolarization ratio of several different vibration modes of the porphyrin ring with the D_{4h} symmetry in the molecular center and the orientation of porphyrin ring on the waveguide surface. This study gave their adsorption orientation angles on the waveguide surface, indicating that the WERS spectrum can detect the adsorption orientation of the surface molecular layer. Although the ZnO waveguide has a high refractive index that can significantly enhance the evanescent field on the waveguide surface, this material will interfere with the Raman vibration response in a range of 440–1150 cm^{-1} by the Raman bands of ZnO itself.[24] Thus, it is in high demand to seek other alternative waveguide materials.

In addition to the thickness and refractive index modulations of the waveguide layer, varying the refractive index of the cladding background can also change the evanescent field intensity of the surface. Hu et al. achieved the reversible adjustment of Raman signal intensity of a 10-nm copper phthalocyanine (CuPc) thin film between the waveguide layer and the cladding by adjusting the refractive index of the liquid cladding layer from 1.00 to 1.33.[27] The Raman scattering signal collected by the objective lens under the waveguide structure was enhanced, whereas the waveguide light collected at the other end of the waveguide weakened, indicating that increasing the refractive index of the cladding can enhance the intensity of the evanescent field penetrating to the surface. With the reversible change of the liquid refractive index, the Raman signal intensity and the output light-guiding intensity also showed a reversible change. In addition, the authors proved that the Raman spectra obtained by this method had good reproducibility and polarization controllability and could easily modulate the evanescent field on the waveguide surface. Reproducibility and polarization controllability are also the unique advantages of WERS over common SERS.

2.1.3 | Strip dielectric waveguide

Compared with the planar dielectric waveguide, the strip waveguide limits the thickness of the waveguide layer and the end-side cross-section area in the horizontal direction. The light-guiding ability of planar dielectric waveguides is worse than that of strip dielectric waveguides, and parts of Raman signals will be lost in the transverse direction.[28] The strip dielectric waveguide can confine the light more in the core layer, as shown in Figure 2B, allowing long-range interaction and facilitating integrated optics. The long-distance interaction of WERS brings high signal collection efficiency and leads to a better enhancement effect than the collection using a traditional confocal Raman microscope.[35] Dhakal et al. discussed the relationship between the specific conversion efficiency η_0 of a single-mode waveguide and the waveguide width,[25] and they found that η_0 first increases and then decreases with the increase of the width. The electric field in the core layer is confined when the width is larger than the optimal value, and the evanescent field on the surface weakens as well. While preparing a strip dielectric waveguide, etching the waveguide layer to limit the transverse width is needed; however, this handling would bring a certain roughness to the waveguide side wall that causes additional energy loss. As a result, a reduction of the effective length of the waveguide and the weakening of the efficiency of Raman scattering will be

inevitable. Therefore, in addition to optimizing the materials and parameters of the waveguide, the innovation of the processing technology is expected during the optimization of the waveguide.

The theory and technology of dielectric waveguides are both mature in telecommunications. They employed the manufacturing process based on the silicon-on-insulator (SOI) that is compatible with the mainstream manufacturing process of comprehensive metal oxide semiconductors (CMOS). SOI is prepared by a high refractive index Si ($n = 3.7$, 785 nm) on the top of the dielectric substrate, followed by the selective etching of the unwanted Si to achieve the core layer. However, this Si-based configuration is inappropriate for WERS. Although the high refractive index of Si can produce a stronger evanescent field on the surface, it is hard to support a pump light below 1 μm because of the strong absorption of Si, and the silicon detector working in visible and near-infrared light exhibits low performance. Moreover, the Raman cross-section is inversely proportional to the fourth power of the excitation wavelength. Thus, a longer wavelength goes against the high-quality Raman scattering signals. Si_3N_4 is an excellent choice as a waveguide material because it is compatible with the CMOS manufacturing process. It has a high refractive index ($n = 2.2$), low loss in visible and near-infrared bands, and almost no interference from autofluorescent signals, which can improve the SNR of collected signals. However, its Raman signal will be excited in the low wavenumber band, especially below 1000 cm^{-1}.[23]

In addition to Si_3N_4,[22,36] Ta_2O_5,[37] TiO_2,[38] and other materials are alternative waveguide materials frequently referred to in recent studies. They all have high refractive indices and Raman conversion efficiencies in the visible light range. Because Raman background signals exist essentially in the amorphous materials,[35] finding suitable crystal materials with an extremely low Raman cross-section is a practical way to achieve highly sensitive WERS. Raza et al.[23] compared the Raman conversion efficiency and background scattering of four waveguide materials as core layers, Al_2O_3, Si_3N_4, Ta_2O_5, and TiO_2, respectively (Figure 2D). The Raman spectra of ethanol on the waveguide layers were recorded (Figure 2E) in comparison with the intrinsic Raman of waveguide materials, and the results indicated that Al_2O_3 provides relatively little vibration information because of the low Raman conversion efficiency, whereas TiO_2 supports poor SNR because of significant background interference and distinguishable vibration information above 1000 cm^{-1}. Si_3N_4 and Ta_2O_5 allow the maximum vibration information and the best SNR because of low background scattering and high signal conversion efficiency. Lee et al. also observed the Raman spectrum of toluene with the largest SNR under a TM polarization mode by analyzing the waveguide structures of Al_2O_3, Si_3N_4, and TiO_2.[21] For strip waveguides, TM polarization has better enhancement performance relative to the TE polarization mode.[25] In TM mode, the discontinuity of the electric field at the interface between the core layer and the upper cladding leads to a higher electric field at the analyte location. Owing to the high aspect ratios of strip waveguides, TM modes endow a larger action area and a higher electric field enhancement.

Dhakal et al. studied WERS spectra of isopropanol on a Si_3N_4 strip dielectric waveguide by subtracting the background of Si_3N_4.[22] The longer interaction distance than linear-type single-mode waveguide between molecules and evanescent field can be achieved by winding a suitable length of waveguide wire into a spiral shape. Si_3N_4 has a broad background emission below 1200 cm^{-1} and a sharp background peak near 2330 cm^{-1}, which can be an internal standard for Raman band normalization.

TiO_2 as the core layer was investigated for Raman signal detection under a pump light of 532 nm by Evans et al.[38] The higher refractive index of TiO_2 brings a higher η_0. Another advantage of using the TiO_2 waveguide is its wavelength flexibility, which can support a broader wavelength range of pump lasers. One advantage of short wavelength pump excitation is that the silicon detector can collect the vibrations of high wavenumbers, such as C–H or O–H vibration in the range of 3000–4000 cm^{-1}, because the Stokes wavelength corresponding to wavenumbers above 3000 cm^{-1} is above 1 μm for 785-nm pump light, beyond the bandwidth edge of a silicon detector.

Besides many WERS studies mainly on optimizing device signal collection efficiency, practical applications using WERS seem few. Here, a summary of recent work on the WERS applications is provided. Makela et al.[39] utilized an AlN strip waveguide to obtain the high SNR Raman spectra of aromatic solvents (benzene, toluene, and anisole) according to its lower loss (0.8 dB/cm) and weaker Raman scattering background than Si_3N_4. Tyndall et al. constructed a 110-nm SiN thin-layer waveguide to explore the WERS of four gaseous organic phosphate compounds in the TM mode,[36] and they explained that the source of characteristic peaks and the subtle differences between spectra are caused by hydrogen bonds. Next, they evaluated the optical properties of several hydrogen-bonded acidic adsorbents using a helical SiN waveguide and estimated their applicability in the detections of gaseous organic phosphorus compounds by WERS spectroscopy.[40] Holmstrom et al. used a Si_3N_4 strip waveguide to realize the Raman detection of trace gas molecules at the concentration of one part per billion (ppb) for the first time.[41] This huge Raman enhancement

not only comes from a large interaction volume but also depends on a thin and optically transparent polymer coating on the waveguide surface that can separate and concentrate specific analytes to 10^8 times. This work shows the applicability of WERS in trace gas sensing and is expected to realize the miniaturization of equipment and the multichannel detections of gas samples.

2.1.4 | Slot dielectric waveguide

The slot dielectric waveguide is composed of two strip waveguides arranged with a certain gap. The parameters considered in the waveguide performance optimization are similar to the strip waveguide. All these impacting factors, such as the waveguide width W (the total width of two strip waveguides and slots), core thickness H, slot width S (Figure 3A), refractive index contrast between the core and the cladding, polarization mode, material selection, and surface roughness, will affect the waveguide enhancement performances.

In slot dielectric waveguides, the enhancement performance of the TE mode is much stronger than the TM mode, which is attributed to a discontinuous electric field distribution in the gap under a TE mode. Under a TM mode, the electric field strength in the gap is much weaker because of the continuity of the electric field,[25] as shown in Figure 3B,C. Compared with the strip waveguide, the width of the gap in the slot waveguide is also an important parameter. As the gap width decreases, the specific conversion efficiency η_0 first increases and then decreases, having an optimal gap width. When the total width is constant, the gap electric field in TE mode increases with the decrease of gap width. However, when the gap is less than the optimal value, the effect of the reduction of the interaction volume is greater than that of the enhancement of the gap electric field, so η_0 shows a downward trend. However, the decrease of gap width has no obvious effect on the gap electric field intensity in TM mode. Compared with the strip dielectric waveguide, the slot waveguide has similar loss[43] but higher conversion efficiency. More electric fields are distributed in the gap rather than in bulk so that the back bottom is lower.[44] The enhancement performance of the slot dielectric waveguide under a TE mode is remarkably better than that of the strip dielectric waveguide of the same size, but there is no apparent difference if the TM mode is applied. In addition, the influence of the total width and refractive index contrast of the waveguide on η_0 is similar to that of the strip waveguide. With the same gap width, η_0 increases first and then decreases, and there is an optimal width as the reduction of the total width. The η_0 of a slot waveguide also rises with the increase of refractive index contrast, and the selection of

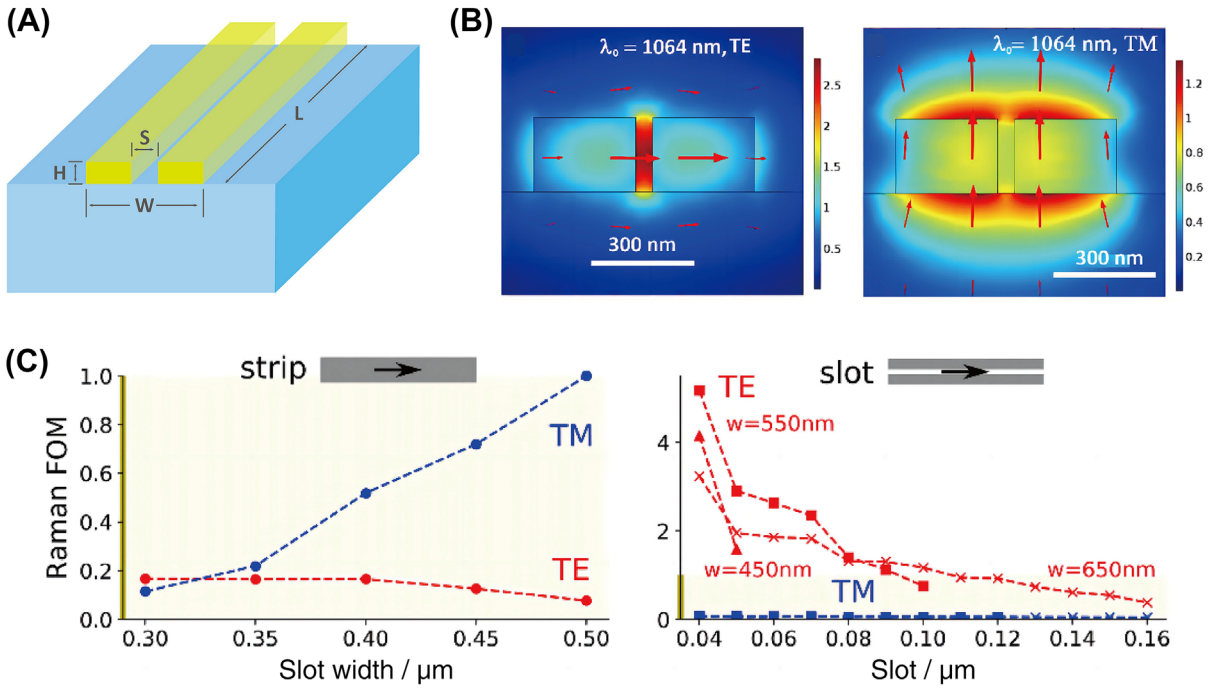

FIGURE 3 (A) Geometrical parameters of slot waveguide: total width W, gap width S, and thickness of the core layer H. (B) Electric field distribution of slot dielectric waveguide in TE and TM modes. Where $S = 50$ nm and $W = 650$ nm. Reproduced with permission.[25] Copyright 2015, The Optical Society. (C) Comparison of the normalized Raman gain coefficient (Raman FOM) of strip and slot waveguides. Reproduced with permission. Copyright 2018,[42] The Optical Society.

waveguide material follows the same trend as that of the strip waveguide.

Dhakal et al. characterized the binding kinetics and surface density of submicron biomolecules on the surface of a waveguide using the near-infrared Raman spectroscopy assisted with Si_3N_4 slot waveguides.[43] Slot dielectric waveguides provided stronger Raman signal intensity and larger SNR than commercial confocal microscopes did and had higher Raman conversion efficiency and lower background scattering than strip dielectric waveguides. Higher conversion efficiency means that high-quality spectral data can be obtained with a shorter integration time, which enables the real-time and efficient detections of biochemical reaction processes on surfaces, as demonstrated by the real-time characterizations of deoxyribonucleic acid (DNA) hybridization and biotin–streptavidin binding processes. This work demonstrates that slot dielectric waveguide is expected to be promising in integrated optics and available for the interaction analysis of biomolecules.

Zhao et al. achieved the Raman response of low-concentration gaseous organic compounds using a 1-cm porous silica functionalized Si_3N_4 slot waveguide.[45] Porous silica can achieve reversible adsorption and adequate enrichment of gaseous molecules. Combined with the large spatial interaction of the slot waveguide and the enhanced electric field at gaps, the Raman detection arrived at a ppm level in a short integration time of 1 s. Liu et al. also used mesoporous silica as a coating in a Si_3N_4 channel waveguide to achieve real-time quantitative detections of low concentrations of nonpolar organic water solutions.[46] These studies demonstrate that the slot dielectric waveguide has a broad application prospect in the real-time and multichannel detection of low-concentration organic and biological molecules.

2.2 | Liquid core waveguide

2.2.1 | Principles and evaluation methods

LCW is a kind of waveguide structure that uses a liquid column or liquid fluid as the core waveguide layer. The refractive index of the liquid core needs to be greater than that of the cladding, so that the light can be effectively confined into the core layer and propagate forward to excite analytes along the way. Both pump light and Raman signal can propagate along the waveguide and can be detected at the output facet. Unlike the high-refractive-index dielectric waveguides mentioned previously, the Raman signal of analytes is not excited by the evanescent field penetrating out of the dielectric surface but excited by the guiding light directly. Similar to the dielectric waveguides, signal contributions to the LCW are mainly from the detection volume increase and long-range excitation/collection (Figure 1B). Therefore, LCWs also have the advantages of small sample volume and uniform excitation, resulting in predictable enhancement factors and highly reproducible Raman signals.[47] Moreover, because LCW is based on bulk excitation, there is no requirement for the specific surface modification for capturing analytes, simplifying the experiment processes.

The performance of LCW can be evaluated either by Raman collection efficiency in dielectric waveguides (Formula 3) or by Raman signal intensity. For a typical backward collection configuration, the Raman intensity can be expressed as[48]

$$I_{LCW} = \frac{P_0}{2\alpha}\gamma\rho\sigma\pi NA\left(1 - e^{-2\alpha L}\right) \quad (3)$$

where γ is the optical coupling efficiency and NA is the numerical aperture of the LCW $\left(NA = \sqrt{n_{core}^2 - n_{clad}^2}\right)$. Because only the Raman scattering falling within the critical angle of the waveguide is collected, the numerical aperture of the waveguide can be considered an appropriate parameter to describe the collection efficiency. Other parameters have the same meaning as Formulas 1 and 2. For an LCW, there is also a preferred waveguide length that supplies the strongest Raman signal, which is similar to the dielectric waveguide. On the premise of detecting a water detection system, the refractive index of the coating layer and the geometric parameters of the waveguide structure are both crucial to limit the light in the core layer as much as possible, which can reduce the transmission loss to increase the efficiency of optical coupling and collection. In the following sections, typical LCW structures will be described.

2.2.2 | Classical LCW

As early as 1972, Wlrafen et al. filled a hollow fused quartz optical fiber ($n = 1.46$) with liquids as a core to detect the Raman signals of the liquids with merit of a long-distance light path.[49] However, because of the high refractive index of the cladding, only the liquid with a refractive index higher than 1.46 can be measured, such as benzene or tetrachloroethylene, and the aqueous solutions are unavailable. To widen the applicability of LCWs for aqueous solutions, cladding materials with a refractive index less than water is needed. The emergence of amorphous fluoropolymer Teflon AF1600[50] and AF2400[51] is a breakthrough for claddings because of their refractive indices being lower than that of water. They

have good light transmittance in aqueous solutions and other transparent liquids with a higher refractive index. More importantly, the Teflon cladding materials can realize the TIR that requires weak light absorption and low optical loss. Meanwhile, these materials can guide a variety of pump wavelength lights to achieve broadband excitation. For a long time, capillary coated with AF2400 has been the mainstream cladding material of an LCW. However, Teflon materials also have some limitations. First, excitation in the visible light range may produce a fluorescent background, which requires additional background correction.[52] Second, the adhesion with common materials is poor. Thus, additional adhesion promoters or additional processing of adhesion materials are needed,[53] which further increases the cost and processing complexity. Developing new low refractive index materials and superhydrophobic cladding materials[54] with an effective refractive index close to the air makes up for the defects of AF2400 on high refractive index and background interference to some extent.

The LCW is an optical element and a liquid flow channel as well, which is convenient to be combined with other characterization systems, such as the coupling of LCW Raman and liquid chromatography,[55,56] so as to realize the integration of separation and detection of multiplex analytes.

2.2.3 | Photonic crystal fiber waveguide

Photonic crystal fiber (PCF) is also called microstructure fiber or porous fiber. The cross-section of its cladding has pores with different arrangements. The size of these pores is usually the same order of magnitude as the wavelength of the incident light and runs through the length of the entire fiber. Thus, it has a complex refractive index distribution. Because of the high air-filling ratio of the cladding, the effective refractive index is relatively low, so the refractive index contrast with the core layer is larger than that of the traditional optical fiber. According to different structures, PCFs are divided into solid-core photonic crystal fibers (SCPCF) and hollow-core photonic crystal fibers (HCPCF), as shown in Figure 4A.[57] The SCPCF has a silicon core with a high refractive index and a diameter of several to tens of microns. Because of the high refractive index contrast of the core and cladding, the light-guiding principle is mainly based on TIR.[61] Similarly, the core layer of HCPCF is a hollow hole structure with a size of tens to hundreds of microns, and the air hole outer structure has strict periodicity. The light-guiding principle of HCPCF is usually based on the photonic band gap effect, which restricts the light to the core layer through the interference effect.[62] The introduction of the hollow core layer destroys its periodic structure and forms a defect state or a local state with a specific bandwidth. As a result, only the light waves with a specific frequency can propagate in the defect region, and the light waves of other frequencies cannot. The photonic band gap effect also depends on the low effective refractive index of the cladding. The photonic band gap of the PCF has extremely low transmission loss and exhibits a nonlinear effect, which can support the long-distance transmission of light and the high-energy pulsed laser transmission, such as stimulated Raman experiment,[63] and also has great application potential in gas and biological sensing. When the hollow core layer is filled with an aqueous solution, as the refractive index contrast between the core layer and the cladding increases, the restriction of light in the core layer is not dominated by the photonic band gap effect anymore, but by the TIR mechanism.[57]

When using Teflon capillary to analyze aqueous solution, because of the small refractive index contrast of the core and cladding, the ability to constrain the light is relatively limited. The hollow core of HCPCF has a cladding layer with a lower effective refractive index, providing a higher refractive index contrast with the core layer, which is conducive to the restriction and propagation of the guiding light in the core layer. Better optical field constraint and lower loss both enable the light to travel a longer distance along the waveguide layer, allowing for a lower pump power on the photo-sensitive samples.[48] However, the discontinuity of pores of the cladding layer or the appearance of defects in HCPCF will inevitably affect the mode propagation.

As for SCPCF, the liquids fill in the porous structure of the claddings, and the silicon core layer displays a higher refractive index than the cladding. For the case of the HCPCF, however, the refractive index contrast between the core and cladding will reduce when the hollow channels of the core and the cladding are both filled with liquid, resulting in the weakening or even disappearance of both the photonic band gap effect and the TIR effect and ultimately seriously affecting the original light guiding ability.[64] In order to limit the light in the core layer as much as possible, we can fill the center holes with a liquid, the cladding holes with air, or close the end of the cladding optical fiber just in case.

2.2.4 | Anti-resonant hollow core waveguide

Because the refractive index of most solid materials is greater than that of water, there are few options to limit the light to an aqueous phase as the waveguide core layer in a TIR way. For this reason, researchers consider direct

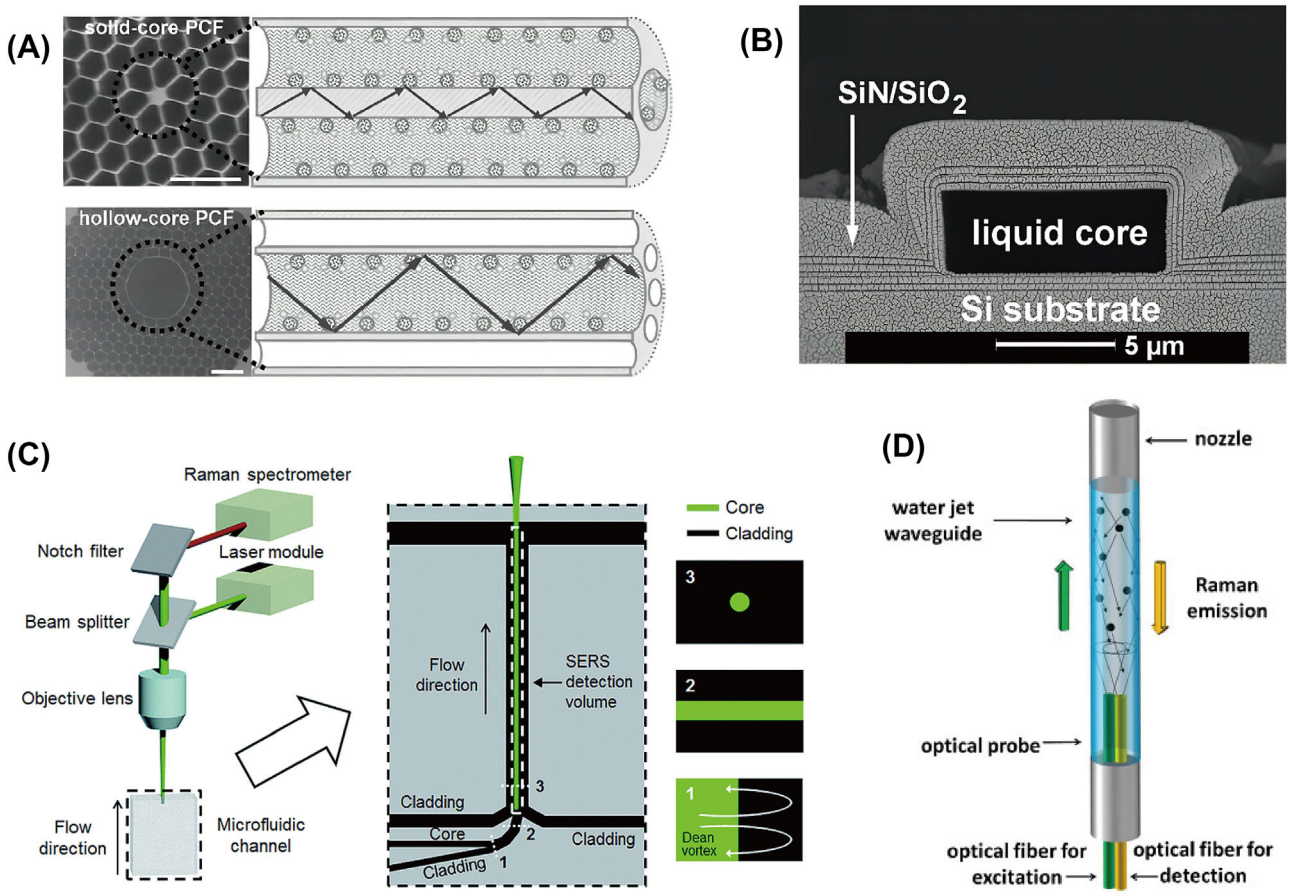

FIGURE 4 (A) Schematic illustrations of the light guiding in the Si core of SCPCF and liquid filled in HCPCF. Reproduced with permission.[57] Copyright 2010, Wiley-VCH. (B) The ARROW cross-section consists of SiN and SiO_2 dielectric layers and a liquid core. Reproduced with permission.[58] Copyright 2007, Applied Physics Letters. (C) Schematic diagram showing the experimental setup and the microfluidic channel design of L^2 waveguide. Reproduced with permission.[59] Copyright 2015, Royal Society Chemistry. (D) Same side of excitation fiber and collection fiber (backward collection configuration) for OJW. Reproduced with permission.[60] Copyright 2015, Elsevier.

light propagation in low refractive index media without relying on the TIR, that is, the anti-resonant waveguide.

One of the typical structures is an anti-resonant reflection optical waveguide (ARROW), which uses the reflection characteristics of multilayer dielectric materials to confine light into the hollow core or the low refractive index core layer (as shown in Figure 4B). ARROWs have been applied for the refractive index and fluorescence sensing.[65] Measor et al. applied the ARROW for the sensitive probe of the Raman signal of R6G, in which an ARROW structure was composed of a Si substrate covered by a SiO_2/SiN composite layer above.[58]

Recently, an anti-resonant waveguide with a hollow core cage was developed.[66] The structure comprises several independent polymer chains arranged in a hexagonal lattice with a high aspect ratio and micron spacing. A hollow core is formed by omitting some central chains in hexagonal lattices. Owing to the modal hybridization and the anti-resonant effect, the mode field can be effectively confined in the core layer, and the diffraction-free propagation of more than 1 cm can be achieved. The most significant advantage of this hollow core anti-resonant waveguide is that it can effectively accelerate the diffusion of gas and liquid to the core because of the open cage structure as cladding, whereas other waveguide structures need to introduce the analyte from the facet. This reduces the difficulty of coupling the sampling system with the waveguide and enables fast and real-time fluid analyses.[67] Cage anti-resonant waveguide structure may be a potential choice in the field of LCW-Raman detection in the future.

2.2.5 | Liquid core/liquid cladding waveguide

In addition to solid materials, low-refractive index liquids can also be used as cladding. The liquid core/liquid

cladding waveguide (L^2 waveguide) is composed of two liquids with different refractive indices (as shown in Figure 4C). At low and medium Reynolds numbers, laminar flow exists between the liquid core and the liquid cladding, resulting in the optical smoothness of the liquid–liquid interface,[68] and the small irregularity in the solid wall of the channel does not propagate to the liquid–liquid interface. The L^2 optical waveguide thereby shows a low optical loss. Meanwhile, the diameter of the liquid and the refractive index contrast of the core and the cladding can be freely controlled by adjusting the flow rate and composition of the liquids, which is a significant advantage of the L^2 waveguides over solid cladding/liquid core waveguides. However, only a few fluids as the cladding can provide a refractive index below that of the water core layer, limiting the scope of applications of the L^2 waveguides. In addition, a large demand for liquid flow also requires a continuous supply of the fluid, which causes the mechanical stability of L^2 waveguides to be inferior to the solid-state waveguides. Nevertheless, flexibility and manufacturing simplicity are two advantageous aspects of L^2 waveguides. Choi et al. developed the L^2 waveguide combined with the SERS detection platform for the sensitive detection of dipicolinic acid.[59] The L^2 waveguide was constructed in a microfluidic device, and the backscattered signals were collected through an objective lens. A silver sol ($n = 1.33$) was the core layer and 2, 2, 2-trifluoroethanol ($n = 1.29$) was the cladding layer, and they were miscible in order to reduce the instability of the laminar flow. It should be noted that the diameter of the core layer can be modified by adjusting the velocity ratios of two liquids. With the increase of the core size, the interaction volume with analytes and the coupling efficiency of light to the core can be increased, whereas the light limitation effect will be reduced in the core. The optimized L^2 waveguide structure achieved a minimum detection concentration of 50 nM for dipicolinic acid.

2.2.6 | Optofluidic jet waveguide

The optofluidic jet waveguide (OJW) is naturally formed by using the jet fluid as the core layer and the air as the cladding.[60] The quasi-static equilibrium between inertia and surface tension leads to the formation of droplets when the flow is at a low speed. Once the liquid velocity is above a certain critical value, the kinetic energy of the fluid will overcome the surface energy of the ejection region, forming continuous jets, as shown in Figure 4D. The jet forms a regular cylinder shape after it flows through a certain length (called the breakup length), and then it is decomposed into water droplets. In this model, a smooth interface exists between the analyte solution ejected from the capillary and the surrounding air as the cladding. As the cladding, air also brings a higher refractive index contrast and a larger numerical aperture than the AF-2400 cladding and the PCF waveguide, which is conducive to restricting the light within the core. In addition, the OJW avoids the requirement for any liquid containers or flow cells, eliminates background signals from the sample containers, and dispenses with complex cleaning steps. The produced stable flow fluid is also valuable for signal reproducibility. Owing to large liquid velocity, the OJWs can be quickly established in the whole system, which is favorable for real-time field detections.

The key factor impacting the sensing performances of the OJWs is the interaction length, that is, the breakup length of the fluid, which has a linear relation with the fluid velocity. A jet with a velocity of about 1.4 m/s can produce a breakup length of about 35 mm.[60] Although the high jet velocity brings stability and smoothness to the liquid column, it requires a large number of samples, which is inapplicable for measuring biological samples. Moreover, the mismatch between the fluid and the end fiber diameter will also lead to additional optical loss.

Persichetti et al. used an OJW to detect common pollutants in water, such as nitrate, sulfate, and benzene.[69] Two side-by-side optical fibers excited the whole fluid and collected backscatter signals. The detection limit of pollutants was about 40 mg/L, which is lower than the minimum standard for the content of related substances in drinking water. In another study, Persichetti et al. integrated the optical fluidic waveguide with the microfluidic system to verify its contribution to Raman and fluorescence sensing.[70] The Raman detection of ethanol was achieved with a LOD of 0.18%. This waveguide exhibited good sensing performance even a low-cost miniature spectrometer was used as a detector. A LOD of Eosin Y was obtained at 33 pM in terms of fluorescence sensing, showing its versatility for spectroscopic detection.

3 | WERS STRUCTURE BASED ON LIMITED-RANGE ENHANCEMENT

Besides long-range enhancement-based WERS that achieves the cumulative amplification of Raman signals by increasing the length of light interacting with molecules, limited-range enhancement-based WERS (Figure 1C,D) attains the amplification of Raman scattering mainly by the enhancement of electromagnetic field interacted with target molecules. This chapter mainly introduces MCW and double MCW (DMCW), between which the evanescent field on the waveguide surface and

the light propagating in the waveguide interacts with molecules severally. Limited-range enhancement-based WERS gives stronger electromagnetic field intensity acting on analytes than long-range enhancement-based WERS at the cost of reduced transmission distance of waveguide light. In the following sections, the structures, principles, strengths, limitations, and applications of two types of waveguides will be described in detail.

3.1 | Metal cladding waveguide

MCW has a metal layer (typically Au or Ag) on one side of the dielectric waveguide and an air or water layer where the analytes are located on the other side. The refractive indices of the claddings are less than the waveguide layer, which allows most of the light-limited into the waveguide layer to form a standing wave. The MCW is also called plasmonic waveguide (PW) because the plasmonic metal is also used as cladding. Here, to distinguish the structures of gold/silver nanowire waveguides in which the plasmonic metals are directly used as the waveguide cores,[71] we note the above configurations as "MCW." The existence of the metal layer above the waveguide layer brings different properties to MCWs compared with the waveguides without metal claddings, such as the penetration depth increase in the cladding and the reduction of stray light interference. In comparison with the single-mode dielectric waveguides or LCWs in which the SERS effect mainly comes from an increase in the interaction volume, MCWs own an attenuated guiding distance because of the intense light absorption of the metal layer. Therefore, the enhanced evanescent field intensity contributes much to Raman enhancement rather than the increased interaction volume in most existing systems.

In MCWs, the thickness of the metal layer is usually dozens of nanometers, which is close to the typical thickness of gold or silver films in surface plasmon resonance (SPR) chips (about 40–50 nm).[72] Thus, MCW shares many similar photophysical properties with SPR. For example, a Kretschmann prism structure is usually used as an optical coupler to meet the wave vector matching condition, as shown in Figure 5A. When the scanning angle exceeds the critical angle of total reflection, TIR occurs between the substrate and the metal layer, and an evanescent wave generates on the surface of the metal layer. The evanescent field at the upper and lower interfaces of the metal layer can be effectively coupled under a proper distance of the metal layer, leading to an enhanced evanescent field and a deeper penetration depth on one side of the waveguide layer. In order to generate a guiding light in the waveguide layer, the wave vector of the incident light is required to meet a phase-matching condition of the guided wave, which produces a narrow and sharp dip similar to that in SPR in the reflection profile (Figure 5B,C). Energy leakage associated with the guided mode involves the absorption and scattering losses of the metal layer, making the guided wave attenuate rapidly along its propagation direction.[74] The metal layer in MCW also brings an "off-resonance" characteristic. When the waveguide mode is failed, most incident light will be confined in the metal layer as a heat decay, resulting in a sharper waveguide resonance peak than SPR.[75,76]

The evanescent field strength on the MCW surface is decided by several factors, for example, the thicknesses of the metal and waveguide layers and their refractive indices. The thickness is usually between 30 and 60 nm for the metal (usually gold or silver) layer. An excessively thin metal layer will reduce the coupling efficiency of light at the metal-dielectric interface, leading to a weakened constraint of the waveguide, which ultimately causes an increase in losses. Correspondingly, a thickness of the metal layer larger than 60 nm will reduce the coupling of the evanescent field at the upper and lower interfaces of the metal layer, giving rise to the enhanced absorption of incident light in the metal layer and the reduction of light reaching the waveguide layer.[77] The thickness of the waveguide layer will affect the distribution of higher-order modes in the waveguide layer and the evanescent field intensity. With an increase in the waveguide thickness, more than one waveguide mode appears, known as higher-order modes, accompanied by the alternative distributions of the electric fields in the waveguide layer (Figure 5D). Generally, only one resonance condition can be detected in a range of 60–75° when the water cladding is used.

Owing to the high reflectivity of the metal layer, the dielectric material as cladding with a high refractive index, like a single-mode dielectric waveguide, is nonessential in MCW. Silicon dioxide,[73,78–81] polymer film,[82] and some functional materials (such as porous material[83] and hydrogel[84]) have been utilized as waveguide materials. For a porous structure waveguide, optimizing the porosity to obtain the best electric field enhancement effect may be a practical way.

McKee et al. first used a Kretschmann prism-based MCW to detect the Raman scattering of a polymer film and a monolayer on the SiO_2 waveguide surface covered with 50-nm gold.[85] The enhancement performances of the TIR-Raman, SPR-Raman, and MCW-Raman were compared (Figure 6A), and the results displayed that MCW-Raman exhibits a stronger enhancement effect by exciting surface molecules with a *p*-polarized light. The scattering of background caused by the prism in MCW-

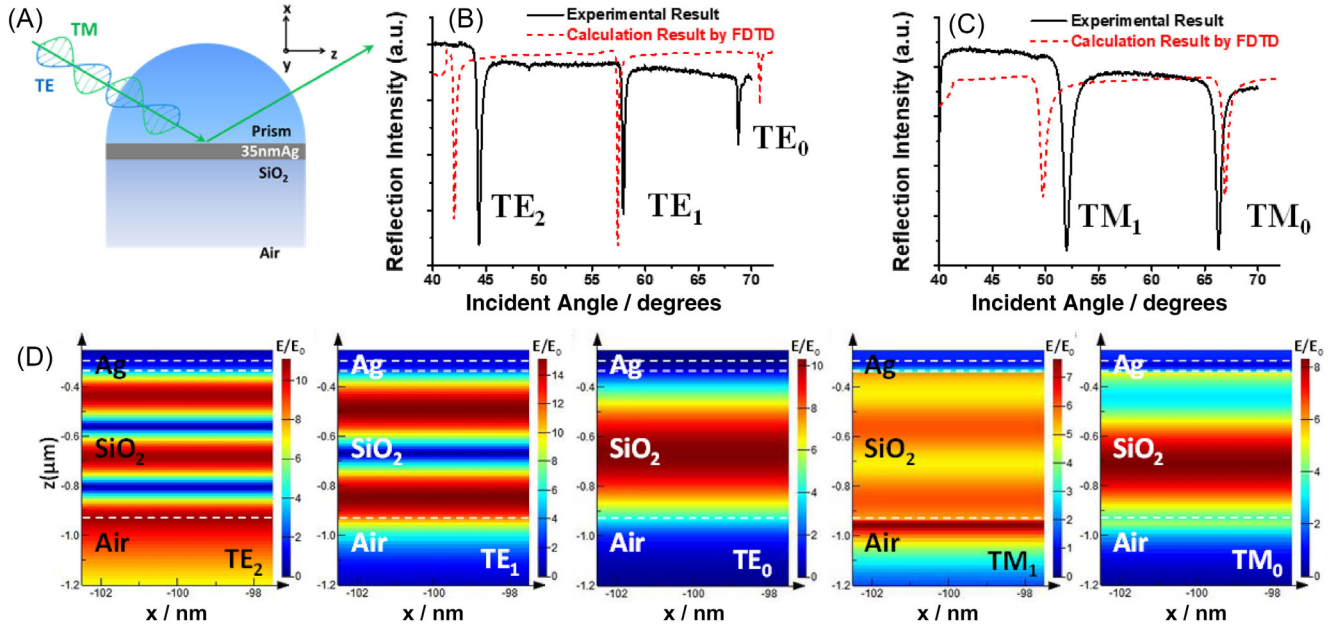

FIGURE 5 (A) Schematic diagram of MCW coupled with prism (K9 glass). The thickness of the silver film is 35 nm, SiO_2 is 600 nm, and the air is used as the cladding. (B) and (C) Resonance angle distribution of MCW in TE and TM modes. (D) The distribution of electric field in SiO_2 layer under different waveguide modes. Reproduced with permission.[73] Copyright 2019, Elsevier.

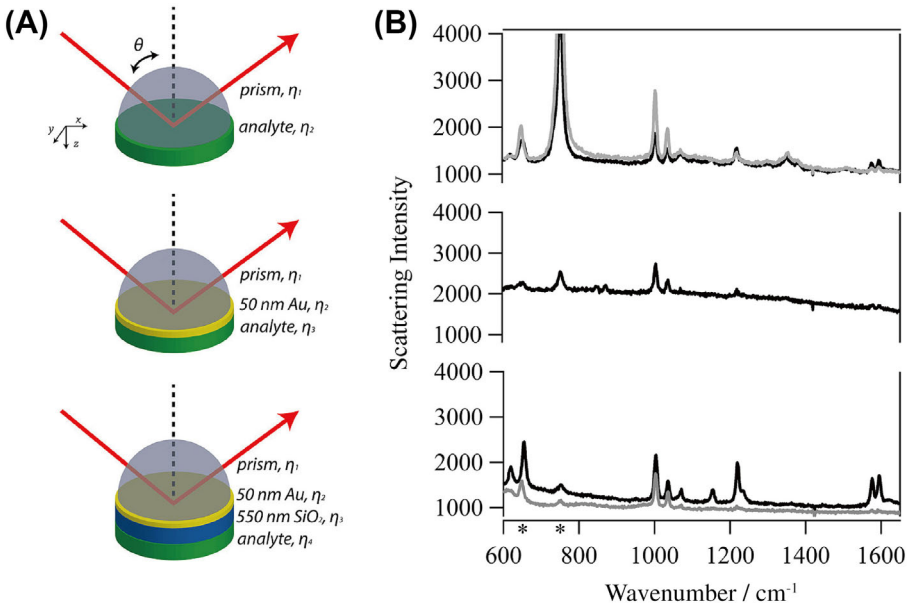

FIGURE 6 (A) Sketch for the experiment configurations of TIR-Raman (top), SPR-Raman (middle), and MCW-Raman (bottom). (B) Corresponding Raman spectra (one-to-one correspondence with the position of each configuration in (A)) at *p*- (black) or *s*- (gray) polarized 785-nm incident light. Reproduced with permission.[85] Copyright 2012, American Chemical Society.

Raman declined significantly in comparison with TIR Raman, as shown in Figure 6B.

In addition to using an MCW structure to modulate the incident light field, how to improve the collection efficiency of scattered light is also worth considering. Chen et al. theoretically studied the radiation of an electric dipole (molecule) in a Kretschmann prism-coupled MCW through an optical reciprocity theorem combined with the Fresnel equation.[86] The electric dipole was located above the waveguide layer of PW, and the azimuth distribution of its radiation was related to the vertical distance to the waveguide surface. When the electric dipole approached the waveguide surface, the radiation power was coupled with the waveguide resonant mode, giving surface directional emission. The radiation power mainly distributes in a specific angular direction in the prism, which is about equal to the resonance angle of the corresponding guided modes at the current incident

wavelengths (as shown in Figure 7A). In contrast, there is a small power proportion of the nondirectional emission radiated into the air. The coupling efficiency between radiation power and waveguide mode decreases rapidly with the distance from the electric dipole to the waveguide surface. Owing to an electric dipole excited by its own space, the detection depth is about 1/e of the penetration depth of the evanescent field, whereas for the electric dipole excited by the guided mode, the detection depth is about one-fourth of the penetration depth. A small part of the radiation power is coupled to the SPR mode of the metal layer, which can be ignored because of the relatively thick waveguide layer. When the target molecules are loaded in the waveguide layer (such as using a porous structure as the light guide layer), the emission efficiency of Raman signals and the coupling efficiency between scattered light and guided modes will be significantly improved, and the directional emission power is stronger than the back emission and nondirectional emission. The penetration depth of the evanescent field in a TM mode is deeper than that in a TE mode. These two modes can be reference signals for each in the same sensing configuration to achieve self-reference directional Raman scattering.

By optimizing the thickness of the metal and waveguide layers, the electric field enhancement factor of over 10-fold can be achieved in MCW. Even so, there is a certain gap in sensitivity between MCW and SERS. The advantages of MCW over SERS lay in the broader application range of surface detections. MCW system can be in conjunction with other surface detection techniques, such as angle-resolved techniques, TIR fluorescence microscopy, and near-field tip scanning techniques (for instance, atomic force microscopy), to learn and analyze the reaction events of surface molecules from more dimensions. To extend the applications of MCW for Raman detections, coupling with LSPR to improve detection sensitivity further is a practical way.

3.2 | Resonant mirror waveguide

A resonance mirror waveguide (RMW) is a leaky waveguide structure composed of a prism with a high

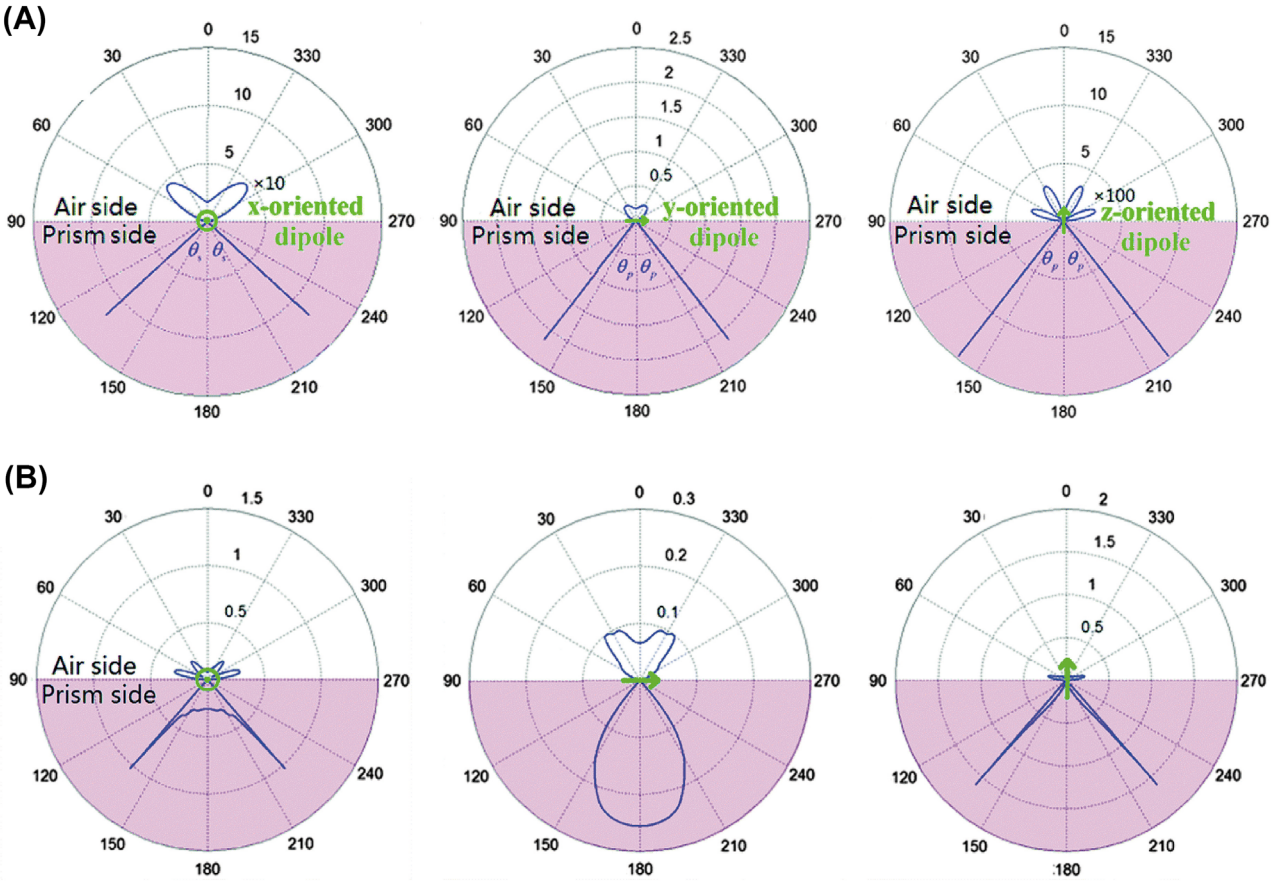

FIGURE 7 Angular distributions of Raman power density from the *x*-, *y*-, and *z*-oriented dipoles located at the waveguide surfaces in MCW (A) and RMW (B). Reproduced with permission.[86] Copyright 2015, Royal Society Chemistry.

refractive index, a dielectric buffer layer with a low refractive index, and a resonant waveguide layer with a high refractive index.[87] When the light reaches the dielectric with a low refractive index through the prism, it will couple with a high refractive index resonance layer, allowing the TIR at the boundary of the resonance layer and generating the evanescent field. Similar to the SPR or MCW configuration, resonance can occur only when the incident angle meets the phase-matching condition under a certain wavelength.

The resonant mirror structure was originally used for biosensors at the interface, which is also a supplement to the SPR scheme.[88] Compared with the MCW structure, RMW has no metal reflector but introduces a medium with a low refractive index as a reflector. Its optical loss is very weak but has a high resonator quality factor Q because no optical absorption by a metal layer exists. Here, Q is equal to the ratio of the resonant wavelength to the FWHM of the resonant peak, which is inversely proportional to the absorption loss of the resonator. The RMW structure can provide strong surface electric field enhancement and has application potential in the field of Raman enhancement. Hu et al. realized the WERS detection using an RMW structure.[89] In this work, MgF_2 was used as a buffer layer with a thickness of 1300–1600 nm, and PMMA was used as a waveguide layer with a thickness of 150–250 nm. The thickness of the waveguide layer supports only a single-mode resonance. Prism coupling was used in the RMW structure, which can couple the incident light into the buffer layer and reorient the Raman scattering through the prism. The Raman signals of CuPc and Cytc were detected to verify the effectiveness of RM-Raman. They also pointed out that the success of this scheme depends on a high-quality film, the accurate determination of resonance conditions, and the efficient collection of Raman scattering. Therefore, it is more challenging to realize Raman signal detections on RMS configurations in comparison with the common MCW and SPR configurations.

Chen et al. studied the Raman directional radiation of RMW.[86] Similar to the MCW, in a Kretschmann prism coupling, the directional radiation efficiency of the electric dipole depends on its orientation and the distance between the electric dipole and the waveguide layer, as presented in Figure 7B. The horizontally oriented electric dipole can couple both TE and TM modes, but the vertically oriented electric dipole couples TM modes only. The directional radiation intensity of RMW was much stronger than that of MCW because of less loss. Different from MCW, the collection efficiencies of horizontal and vertical dipoles on the prism side were similar, with no orientation selectivity.[90] The directional emissions of the scattering light in both MCW and RMW were assigned to the limited-range enhancement according to the SERS enhancement mechanism.

3.3 | Double metal cladding waveguide

DMCW comprises a waveguide layer and the upper and lower metal layers (Figures 1D and 8A), in which one metal layer is as thick as hundreds of nanometers, whereas the other metal layer is usually only dozens of nanometers.[91] Silver is usually selected for the metal layers with good reflection performance. Because of Ag layers, the DMCW is also considered a PW. However, because of the introduction of metal mirrors as the claddings on both sides, the optical properties of DMCW are somewhat different from the MCW mentioned above. The role of the thick silver layer is to reflect the light in the guiding mode without transmission effectively. The thin silver layer is used to effectively couple the incident light into the waveguide layer, which is also a reflector to limit the light in the waveguide layer as in the MCW. The overall structure is a symmetrical metal–waveguide–metal sandwich structure, in which the effective refractive index of the waveguide layer tends to zero. The high-intensity guided modes exist in the guiding wave layer as a standing wave, and the guiding light is effectively confined in the waveguide layer. The thickness of the waveguide layer can be adjusted from a micron scale to a millimeter scale. The number of guided modes increases with the waveguide thickness, and a millimeter-thickness waveguide will produce thousands of guided modes, supporting thousands of periodically distributed electric field enhancement regions, which can be applicable for sensing detection[92] and Raman enhancement.[91,93–95]

Uniqueness in the DMCW structures makes them different from the MCWs. First, for the relatively thick DMCW chips, the excitation of ultra-high-order modes is independent of light polarization because hundreds to thousands of resonant modes are distributed within a limited angle scanning range, making the corresponding resonant angles of TE and TM modes almost overlapping (Figure 8A,B). Meanwhile, because many guided modes are distributed in each angle range, the free space optical coupling technology can be realized in DMCW by directly focusing a laser on the analytes by an objective lens without relying on prism coupling and angle/wavelength scanning to meet specific phase-matching conditions. The converging laser beam directly irradiating the chip surface can also simultaneously excite

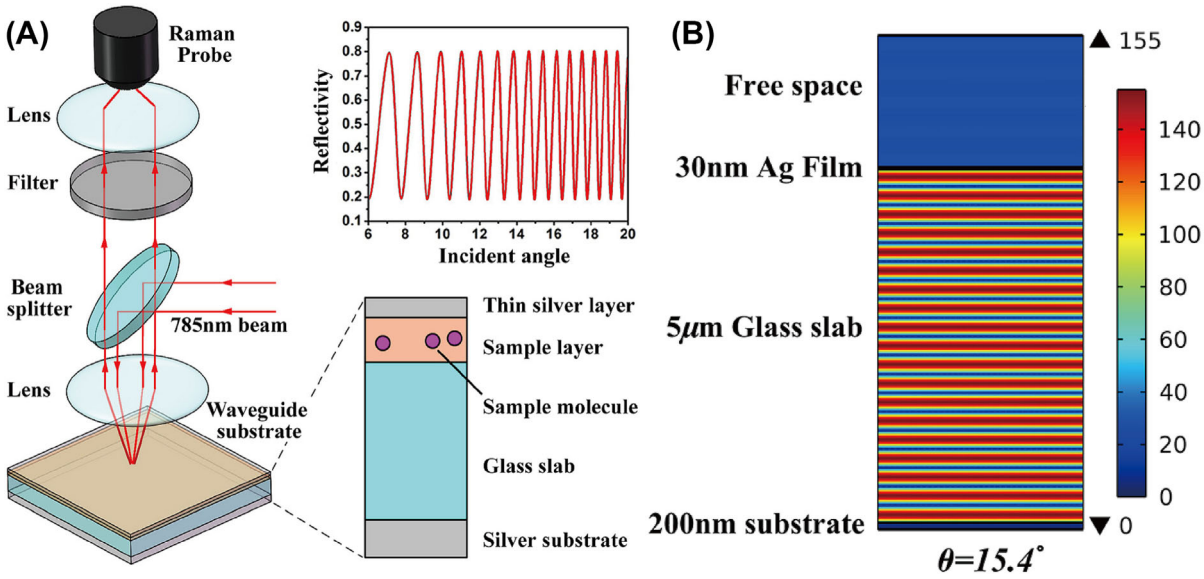

FIGURE 8 (A Experimental setup of the DMCW enhanced Raman scattering scheme and experimentally detected reflection spectrum of the DMCW chip. (B) Distribution of the electric field amplitude|E| for TE mode with θ = 15.4°. Reproduced with permission.[91] Copyright 2014, Applied Physics Letters.

several oscillation modes in the guided light layer, making the enhancement distribution more uniform, as shown in Figure 8B. Second, the light in the DMCW structure is basically confined in the waveguide layer. So, it is unnecessary to capture analytes or enrich them on a specific surface, which differs from the evanescent field-based waveguide structures, such as MCW and RMW. In addition, the waveguide layer of the DMCW has a large volume, which can effectively expand the detection area and achieve an excellent overall enhancement performance. Third, the DMCW structure is easy to fabricate. Glass sheets or polymer coatings can be available for the supporting waveguide layers without high demands on those precise thin film processing technologies.

However, DMCW also displays limitations in some aspects. First, DMCW belongs to a bulk phase-enhanced structure, similar to LCW. It has no surface selectivity and is feeble in analyzing binding events between the receptor adsorbed on the surfaces and the analytes. Second, the larger thickness of the waveguide layer and the existence of metal as a reflector will also increase the loss of the scattering lights, and the collection efficiency in free space may be lower than that of other waveguide structures. Third, the electric field of the DMCW structure is mainly limited to a high refractive index part of the waveguide layer. Because the refractive index of water is lower than most dielectric materials supporting waveguide modes, detections in an aqueous phase need to be solved further.

Xu et al. studied the distribution of resonance angle and electric field of three different DMCW structures for the Raman enhancement effect.[91] Two of the three DMCWs have different thickness waveguide layers (5 and 170 μm), and another one is a single metal cladding structure without a thick silver layer below (170 μm thickness waveguide layer). The excitation light was incident from one side of the thin silver layer. For the DMCW structure with a 5-μm waveguide, the resonant peak distribution is sparse and polarization-selective (the resonant angles of TE and TM modes are distinguishable). The distribution density of resonance peaks for the DMCW structure with a 170-μm waveguide layer is relatively high, accompanied by the nonpolarization selectivity. A broad distribution density of resonant peaks was observed for the structure without a thick silver layer. However, the reflectivity under resonance conditions increases significantly and shows polarization-selective. The enhancement effect of the DMCW structure is better than that of a single metal-clad waveguide without a thick silver layer.

Although the increase in the waveguide layer thickness can support many higher-order waveguide modes, the field intensity corresponding to each mode will decrease. Therefore, a compromise should be made between mode strength and density in order to achieve the best enhancement effect. Xu et al. explored a new strategy to double the mode density while keeping the thickness of the conductive layer unchanged.[94] A new

TABLE 1 Summary of some assessment indices of different types of WERS.

Waveguide type	Features			
	Processing difficulty	Mechanical stability	Required sample volume	Extensibility
Slab dielectric waveguide	++	+++	+	+++
Strip dielectric waveguide	+++	+++	+	+++
Slot dielectric waveguide	+++	+++	+	+++
Classical liquid core waveguide	+	++	+	+
Photonic crystal waveguide	++	++	+	+
Antiresonance hollow core waveguide	++	++	+	+
Liquid core/liquid cladding waveguide	+++	+	+++	+
Optofluidic jet waveguide	+	+	+++	+
Metal cladding waveguide	++	+++	+	+++
Resonant mirror waveguide	++	+++	+	+++
Double metal cladding waveguide	+	+++	++	+

double cavity DCMW structure was designed, in which another metal film was inserted to divide the waveguide layer into two, whereas the sample was only involved in one part. Two cavities are similar in structure, and their bound states interfere with each other, resulting in mode splitting, which can double the mode density of the DCMW without changing the volume of the conductive layer. It is found that the electric field is more robust in the cavity with a high refractive index. So, the electric field can be more concentrated in the interested region by adjusting the refractive index contrast of two DMCW cavities.

4 | CONCLUSION AND OUTLOOK

4.1 | Summary of WERS

We listed five types of WERS and stated their principles and structures, and two of them are based on the evanescent field excitation and the other three are according to direct excitation by light propagated within the waveguide mediums. Table 1 compares their features on the processing difficulty, mechanical stability, required sample volume, and extensibility.

The WERS is an important supplement to the SERS technology, which can achieve complementary advantages in the following aspects.

1. High sensitivity can be achieved. The single-mode dielectric waveguide and LCW provide long-distance and large-volume molecule-electric field interaction to realize the cumulative amplification of Raman signals. MCW and RMW supply an evanescent field on the surface with a high enhancement factor and a deep penetration distance. The reasonable waveguide structure designs and the low-loss waveguide materials illuminated by mature manufacturing technology promise a high sensitivity comparable to the LSPR-dominated SERS.
2. Photodamage is avoided. The optical path of the pump light and the scattering light in the dielectric waveguide and the cladding waveguide do not directly pass through analytes. A much lower pump light power applied in the LCW will achieve a comparable detection effect as the conventional Raman, which effectively avoids photodamage or additional photothermal reactions that often happen under direct pump light irradiation with large laser power. In addition, with the amplification effect from SERS hot spots, the plasmon-coupled waveguides excited under a small incident light power can generate a strong local electric field. Plasmonic hot spots in SERS will amplify the incident and the scattering electric fields and will also amplify the ohmic loss associated with free electron oscillation, resulting in an increased temperature in the hot spots. Although this is a major advantage of plasmons in nanotemperature measurement,[96] during Raman detection, the appearance of metal may lead to the thermal denaturation of the sample and the thermal deformation of the plasmonic structure. Also, it may lead to a charge transfer to surface molecules

caused by high-energy hot carriers, which may lead to desorption, photolysis, or photobleaching reactions. In the waveguide structures, the amplification of the electric field is based on a light interference effect, which is independent of the oscillation of free charges.

3. Applicable for large molecule measurements. Compared with the plasmonic structures, the waveguide structures can provide a uniform electric field region in a large area, although the intensity per unit area or volume might be less than the extreme enhancement regions of the plasmonic gaps, tips, or edges. However, regarding biological molecule detections, more uniform enhancement may be preferable from the view of the universality of analytes.[13] Meanwhile, the waveguide structure can provide a larger hot spot space than the plasmonic nanoparticle surface or nano-cavity produced by aggregation of a plasmonic nanostructure. Therefore, compared with the plasmonic nanostructures with an effective detection range of only a few nanometers, the waveguide structure is more suitable for detecting biological macromolecules.
4. Dielectric surface blocks unwanted hot electrons and is more flexible for surface modification during surface analysis. Molecules detected in the dielectric-supported waveguide or plasmonic SERS are required to interact with the evanescent field on the surface, which requires the analytes to be closely positioned on the substrate surface first. Such close contact may bring unexpected impacts on the analyses of peak positions and relative intensity. Biological molecules may even be denatured and inactivated because of the formation of characteristic chemical bonds, such as noble metal and disulfide bonds, which may confuse the spectral profiles and bring troubles to Raman peak assignments. The dielectric surface is chemically inserted with few hot electrons joining in, which is favorable for achieving instinct Raman signals. The surface of the dielectric waveguide is more reliable relative to the metal surface for surface chemical/physical modifications, especially for in vitro reconstruction systems, for example, the lipid support bilayer.[97] The chemical modification strategy of a waveguide surface is systematically described in the previous review paper.[20]
5. Waveguide-Raman allows both *s*- and *p*-polarizations for excitation. Compared with SERS, waveguide-Raman enables a more comprehensive study of the Raman polarization tensors of molecules and the polarization information (such as molecular orientation), whereas SERS is more sensitive to dipoles perpendicular to the surface.
6. Wide wavelength selection. For many finely regulated plasmonic nanostructures, there are usually strict requirements for the working wavelength and bandwidth to match the corresponding plasmon resonance. In the waveguide structure, the working bandwidth is only related to the optical transparent band of the dielectric material, and the working bandwidth is generally broad. (However, the interband transition is nonnegligible in MCW when gold is used as a metal layer). The common waveguide structure can usually support most of the working wavelengths in the visible range.
7. The size of the waveguide structure can be accurately adjusted during preparation, and the substrates are easy to store and reuse. In addition, easy miniaturization and integration are also two main advantages over plasmonic SERS substrates.

4.2 | Outlook of WERS

In the future, WERS technology can be combined with other Raman enhancement technologies. The substrates with reasonable designs are expected to provide high sensitivity comparable with SERS. The quality factor is suggested to be further increased by the coupling of resonance in waveguides and in dielectric cavities,[19] which can reduce the light attenuation and achieve high detection sensitivity in the absence of plasmon. Waveguide structures integrated with the tip-enhanced Raman scattering (TERS) technology are promising. The existence of a waveguide structure can provide an enhanced evanescent field, improving the detection sensitivity of TERS.[98] This light coupler can also avoid intense pump light irradiating at the tip detection area, reducing background interferences. WERS can also be combined with other detection technologies, such as electrochemical Raman and time-resolved Raman, and has valuable applications in the characterization of catalytic processes and biological events.

At the present stage, the theoretical framework of WERS is mainly complete. However, it is now in the proof-of-concept stage in terms of practical research, mainly utilizing some simple small molecules to verify the feasibility of the WERS strategy. The next phase of research could mainly focus on the application stage. The flexibility of some WERS structures, especially single-mode dielectric waveguides, makes them easy to be integrated with a very small space and with other 2D devices to obtain a complete on-chip detection scheme. An integrated chip that combines signal excitation, detection, and data analysis is a key development direction in the field of biomedical sensors in the future. The realization

of this technology is expected to achieve real-time and position, sensitive and reliable Raman detection of clinical samples without the requirement for complex and expensive Raman detection devices. At the same time, the development of data processing methods based on machine learning and deep learning algorithms also helps to separate the spectral information of interested components from multicomponent and complicated samples. Combined with big data analysis technology and Internet of Things (IoT) technology, the relevant information of the chip carriers can be quickly analyzed and uploaded into the database, suggesting the best diagnostic and treatment plan in the first time.

ACKNOWLEDGEMENTS

We thank the support of National Natural Science Foundation of China NSFC (Nos. 21827805, 21873039, and 22173035), Fundamental Research Funds for the Central Universities, Science and Technology Development Program Projects of Jilin Province (20220101046JC), Opening Project of the State Key Laboratory of Applied Optics (SKLAO2021001A14), and Interdisciplinary Integration Innovation Project of Jilin University (JLUXKJC2020106). We appreciate Dr. Zhimei Qi, Aerospace Information Research Institute, Chinese Academy of Science, Beijing; Dr. Yu Tian from Changchun Institute of Applied Chemistry, Chinese Academy of Sciences; Dr. Hailong Wang from TAN KAH KEE Innovation Laboratory, Xiamen; and Dr. Yuejiao Gu and Dr. Haibo Li from China Academy of Engineering Physics, Mianyang, for their early work and helpful discussion.

ORCID

Weiqing Xu https://orcid.org/0000-0002-1947-317X
Shuping Xu https://orcid.org/0000-0002-6216-6175

REFERENCES

[1] L. Tang, J. Li, *ACS Sens.* **2017**, *2*, 857.
[2] Z. Zhang, H. Wang, Z. Chen, X. Wang, J. Choo, L. Chen, *Biosens. Bioelectron.* **2018**, *114*, 52.
[3] E. Benito-Pena, M. G. Valdes, B. Glahn-Martinez, M. C. Moreno-Bondi, *Anal. Chim. Acta* **2016**, *943*, 17.
[4] Q. Yang, J. Li, X. Wang, H. Peng, H. Xiong, L. Chen, *Biosens. Bioelectron.* **2018**, *112*, 54.
[5] Y. Xu, P. Bai, X. Zhou, Y. Akimov, C. E. Png, L. Ang, W. Knoll, L. Wu, *Adv. Opt. Mater.* **2019**, *7*, 1801433.
[6] T. H. Lee, D. J. Hirst, K. Kulkarni, M. P. Del Borgo, M. I. Aguilar, *Chem. Rev.* **2018**, *118*, 5392.
[7] H. Altug, S. H. Oh, S. A. Maier, J. Homola, *Nat. Nanotechnol.* **2022**, *17*, 5.
[8] M. Fleischmann, P. J. Hendra, A. J. McQuillan, *Chem. Phys. Lett.* **1974**, *26*, 163.
[9] I. Bruzas, W. Lum, Z. Gorunmez, L. Sagle, *Analyst* **2018**, *143*, 3990.
[10] J. F. Li, Y. J. Zhang, S. Y. Ding, R. Panneerselvam, Z. Q. Tian, *Chem. Rev.* **2017**, *117*, 5002.
[11] C. Zhan, X.-J. Chen, J. Yi, J.-F. Li, D.-Y. Wu, Z.-Q. Tian, *Nat. Rev. Chem.* **2018**, *2*, 216.
[12] J. Langer, D. Jimenez de Aberasturi, J. Aizpurua, R. A. Alvarez-Puebla, B. Auguie, J. J. Baumberg, G. C. Bazan, S. E. J. Bell, A. Boisen, A. G. Brolo, J. Choo, D. Cialla-May, V. Deckert, L. Fabris, K. Faulds, F. J. Garcia de Abajo, R. Goodacre, D. Graham, A. J. Haes, C. L. Haynes, C. Huck, T. Itoh, M. Kall, J. Kneipp, N. A. Kotov, H. Kuang, E. C. Le Ru, H. K. Lee, J. F. Li, X. Y. Ling, S. A. Maier, T. Mayerhofer, M. Moskovits, K. Murakoshi, J. M. Nam, S. Nie, Y. Ozaki, I. Pastoriza-Santos, J. Perez-Juste, J. Popp, A. Pucci, S. Reich, B. Ren, G. C. Schatz, T. Shegai, S. Schlucker, L. L. Tay, K. G. Thomas, Z. Q. Tian, R. P. Van Duyne, T. Vo-Dinh, Y. Wang, K. A. Willets, C. Xu, H. Xu, Y. Xu, Y. S. Yamamoto, B. Zhao, L. M. Liz-Marzan, *ACS Nano* **2020**, *14*, 28.
[13] L. A. Lane, X. Qian, S. Nie, *Chem. Rev.* **2015**, *115*, 10489.
[14] C. Zong, M. Xu, L. J. Xu, T. Wei, X. Ma, X. S. Zheng, R. Hu, B. Ren, *Chem. Rev.* **2018**, *118*, 4946.
[15] S. Nie, S. R. Emory, *Science* **1997**, *275*, 1102.
[16] K. Kneipp, Y. Wang, H. Kneipp, M. S. Feld, L. T. Perelman, I. Itzkan, R. R. Dasari, *Phys. Rev. Lett.* **1997**, *78*, 1667.
[17] P. Wang, L. Zhu, B. Zhao, *Chin. J. Light Scattering* **2023**, *35*, 150.
[18] K. A. Willets, *Chem. Soc. Rev.* **2014**, *43*, 3854.
[19] I. Alessandri, J. R. Lombardi, *Chem. Rev.* **2016**, *116*, 14921.
[20] M. A. Ettabib, A. Marti, Z. Liu, B. M. Bowden, M. N. Zervas, P. N. Bartlett, J. S. Wilkinson, *ACS Sens.* **2021**, *6*, 2025.
[21] W. Lee, P. Munoz-Galindo, I. Hegeman, Y.-S. Yong, M. Dijkstra, S. M. Garcia-Blanco, H. L. Offerhaus, *Osa Continuum* **2020**, *3*, 1322.
[22] A. Dhakal, A. Z. Subramanian, P. Wuytens, F. Peyskens, N. Le Thomas, R. Baets, *Opt. Lett.* **2014**, *39*, 4025.
[23] A. Raza, S. Clemmen, P. Wuytens, M. de Goede, A. S. K. Tong, N. Le Thomas, C. Liu, J. Suntivich, A. G. Skirtach, S. M. Garcia-Blanco, D. J. Blumenthal, J. S. Wilkinson, R. Baets, *Opt. Express* **2019**, *27*, 23067.
[24] J. S. Kanger, C. Otto, M. Slotboom, J. Greve, *J. Phys. Chem.* **1996**, *100*, 3288.
[25] A. Dhakal, A. Raza, F. Peyskens, A. Z. Subramanian, S. Clemmen, N. Le Thomas, R. Baets, *Opt. Express* **2015**, *23*, 27391.
[26] A. Dhakal, F. Peyskens, S. Clemmen, A. Raza, P. Wuytens, H. Zhao, N. Le Thomas, R. Baets, *Interface Focus.* **2016**, *6*, 20160015.
[27] D.-B. Hu, Z.-M. Qi, *J. Phys. Chem. C* **2013**, *117*, 16175.
[28] M. A. Ettabib, Z. Liu, M. N. Zervas, J. S. Wilkinson, *Opt. Express* **2020**, *28*, 37226.
[29] Z. Wang, S. J. Pearce, Y.-C. Lin, M. N. Zervas, P. N. Bartlett, J. S. Wilkinson, *Appl. Spectrosc.* **2016**, *70*, 1384.
[30] Z. Wang, M. N. Zervas, P. N. Bartlett, J. S. Wilkinson, *Opt. Lett.* **2016**, *41*, 4146.
[31] Y. Levy, C. Imbert, J. Cipriani, S. Racine, R. Dupeyrat, *Opt. Commun.* **1974**, *11*, 66.

[32] J. F. Rabolt, R. Santo, J. D. Swalen, *Appl. Spectrosc.* **1980**, *34*, 517.
[33] D. S. Walker, H. W. Hellinga, S. S. Saavedra, W. M. Reichert, *J. Phys. Chem.* **1993**, *97*, 10217.
[34] J. S. Kanger, C. Otto, *Appl. Spectrosc.* **2003**, *57*, 1487.
[35] J. Michon, D. Kita, J. Hu, *J. Opt. Soc. Am. B* **2020**, *37*, 2012.
[36] N. F. Tyndall, T. H. Stievater, D. A. Kozak, K. Koo, R. A. McGill, M. W. Pruessner, W. S. Rabinovich, S. A. Holmstrom, *Opt. Lett.* **2018**, *43*, 4803.
[37] D. A. Coucheron, D. N. Wadduwage, G. S. Murugan, P. T. C. So, B. S. Ahluwalia, *IEEE Photon. Technol. Lett.* **2019**, *31*, 1127.
[38] C. C. Evans, C. Liu, J. Suntivich, *ACS Photon.* **2016**, *3*, 1662.
[39] M. Makela, P. Gordon, D. Tu, C. Soliman, G. L. Cote, K. Maitland, P. T. Lin, *Anal. Chem.* **2020**, *92*, 8917.
[40] N. F. Tyndall, T. H. Stievater, D. A. Kozak, M. W. Pruessner, B. J. Roxworthy, W. S. Rabinovich, C. A. Roberts, R. A. McGill, B. L. Miller, E. Luta, M. Z. Yates, *Acs Sens.* **2020**, *5*, 831.
[41] S. A. Holmstrom, T. H. Stievater, D. A. Kozak, M. W. Pruessner, N. Tyndall, W. S. Rabinovich, R. A. McGill, J. B. Khurgin, *Optica* **2016**, *3*, 891.
[42] D. M. Kita, J. Michon, S. G. Johnson, J. Hu, *Optica* **2018**, *5*, 1046.
[43] A. Dhakal, P. C. Wuytens, F. Peyskens, K. Jans, N. Le Thomas, R. Baets, *ACS Photon.* **2016**, *3*, 2141.
[44] A. Dhakal, P. Wuytens, A. Raza, N. Le Thomas, R. Baets, *Materials* **2017**, *10*, 140.
[45] H. Zhao, B. Baumgartner, A. Raza, A. Skirtach, B. Lendl, R. G. Baets, *Opt. Lett.* **2020**, *45*, 447.
[46] Z. Liu, H. Zhao, B. Baumgartner, B. Lendl, A. Stassen, A. Skirtach, N. Le Thomas, R. Baets, *Opt. Lett.* **2021**, *46*, 1153.
[47] D. Qi, A. J. Berger, *Appl. Spectrosc.* **2004**, *58*, 1165.
[48] F. Eftekhari, J. Irizar, L. Hulbert, A. S. Helmy, *J. Appl. Phys.* **2011**, *109*, 113104.
[49] G. E. Walrafen, J. Stone, *Appl. Spectrosc.* **1972**, *26*, 585.
[50] R. Altkorn, I. Koev, R. P. Van Duyne, M. Litorja, *Appl. Optim.* **1997**, *36*, 8992.
[51] J. H. Lowry, *Opt. Eng.* **1992**, *31*, 1982.
[52] M. J. Pelletier, R. Altkorn, *Appl. Spectrosc.* **2000**, *54*, 1837.
[53] R. Manor, A. Datta, I. Ahmad, M. Holtz, S. Gangopadhyay, T. Dallas, *IEEE Sens. J.* **2003**, *3*, 687.
[54] K. Du, I. Wathuthanthri, J. Ding, C.-H. Choi, *Appl. Phys. Lett.* **2018**, *113*, 143701.
[55] B. J. Marquardt, P. G. Vahey, R. E. Synovec, L. W. Burgess, *Anal. Chem.* **1999**, *71*, 4808.
[56] R. J. Dijkstra, G. J. Slooten, A. Stortelder, J. B. Buijs, F. Ariese, U. A. T. Brinkman, G. Gooijer, *J. Chromatogr. A* **2001**, *918*, 25.
[57] Y. Han, S. Tan, M. K. Oo, D. Pristinski, S. Sukhishvili, H. Du, *Adv. Mater.* **2010**, *22*, 2647.
[58] P. Measor, L. Seballos, D. Yin, J. Z. Zhang, E. J. Lunt, A. R. Hawkins, H. Schmidt, *Appl. Phys. Lett.* **2007**, *90*, 211107.
[59] J. Choi, K. S. Lee, J. H. Jung, H. J. Sung, S. S. Kim, *RSC Adv.* **2015**, *5*, 922.
[60] G. Persichetti, G. Testa, R. Bernini, *Sens. Actuators B* **2015**, *207*, 732.
[61] J. C. Knight, T. A. Birks, P. S. J. Russell, D. M. Atkin, *Opt. Lett.* **1996**, *21*, 1547.
[62] J. C. Knight, J. Broeng, T. A. Birks, P. S. J. Russell, *Science* **1998**, *282*, 1476.
[63] F. Benabid, J. C. Knight, G. Antonopoulos, P. S. J. Russell, *Science* **2002**, *298*, 399.
[64] Y. Zhang, C. Shi, C. Gu, L. Seballos, J. Z. Zhang, *Appl. Phys. Lett.* **2007**, *90*, 193504.
[65] X. Fan, I. M. White, *Nat. Photonics* **2011**, *5*, 591.
[66] C. Jain, A. Braun, J. Gargiulo, B. Jang, G. Li, H. Lehmann, S. A. Maier, M. A. Schmidt, *ACS Photon.* **2018**, *6*, 649.
[67] J. Kim, B. Jang, J. Gargiulo, J. Buerger, J. Zhao, S. Upendar, T. Weiss, S. A. Maier, M. A. Schmidt, *Anal. Chem.* **2021**, *93*, 752.
[68] D. B. Wolfe, R. S. Conroy, P. Garstecki, B. T. Mayers, M. A. Fischbach, K. E. Paul, M. Prentiss, G. M. Whitesides, *Proc. Nat. Acad. Sci. U.S.A.* **2004**, *101*, 12434.
[69] G. Persichetti, R. Bernini, *Talanta* **2016**, *155*, 145.
[70] G. Persichetti, I. A. Grimaldi, G. Testa, R. Bernini, *Lab. Chip.* **2017**, *17*, 2631.
[71] Y. Huang, Y. Fang, Z. Zhang, L. Zhu, M. Sun, *Light Sci. Appl.* **2014**, *3*, e199.
[72] S. A. Meyer, E. C. Le Ru, P. G. Etchegoin, *Anal. Chem.* **2011**, *83*, 2337.
[73] Y. Tian, H. Wang, W. Xu, Y. Liu, S. Xu, *Sens. Actuators B* **2019**, *280*, 144.
[74] Z. Zhang, Z.-M. Qi, *Chin. J. Anal. Chem.* **2010**, *38*, 1538.
[75] M. Zourob, S. Mohr, B. J. T. Brown, P. R. Fielden, M. McDonnell, N. J. Goddard, *Sens. Actuators B* **2003**, *90*, 296.
[76] A. Abbas, M. J. Linman, Q. Cheng, *Sens. Actuators B* **2011**, *156*, 169.
[77] G. Zheng, J. Cong, L. Xu, J. Wang, *Appl. Phys. Express* **2017**, *10*, 042202.
[78] Y. Tian, H. Wang, Y. Geng, L. Cong, Y. Liu, W. Xu, S. Xu, *Photonics Res.* **1850**, *2020*, 8.
[79] Y. Tian, W. Xu, K. Ma, L. Cong, Y. Shen, X. Han, C. Liang, L. Liang, G. Qi, Y. Jin, S. Xu, *J. Phys. Chem. Lett.* **2021**, *12*, 10720.
[80] Y. Gu, S. Xu, H. Li, S. Wang, M. Cong, J. R. Lombardi, W. Xu, *J. Phys. Chem. Lett.* **2013**, *4*, 3153.
[81] X. Kan, C. Yin, J. Wu, B. Li, Q. Han, *J. Raman Spectrosc.* **2019**, *50*, 908.
[82] S. Wang, Z. Wu, L. Chen, Y. Gu, H. Wang, S. Xu, W. Xu, *J. Phys. Chem. C* **2015**, *119*, 24942.
[83] C. Fu, Y. Gu, Z. Wu, Y. Wang, S. Xu, W. Xu, *Sens. Actuators B* **2014**, *201*, 173.
[84] Q. Zhang, Y. Wang, A. Mateescu, K. Sergelen, A. Kibrom, U. Jonas, T. Wei, J. Dostalek, *Talanta* **2013**, *104*, 149.
[85] K. J. McKee, M. W. Meyer, E. A. Smith, *Anal. Chem.* **2012**, *84*, 9049.
[86] C. Chen, J.-Y. Li, L. Wang, D.-F. Lu, Z.-M. Qi, *Phys. Chem. Chem. Phys.* **2015**, *17*, 21278.
[87] H. N. Daghestani, B. W. Day, *Sensors (Basel)* **2010**, *10*, 9630.
[88] R. Cush, J. M. Cronin, W. J. Stewart, C. H. Maule, J. Molloy, N. J. Goddard, *Biosens. Bioelectron.* **1993**, *8*, 347.
[89] D.-B. Hu, C. Chen, Z.-M. Qi, *J. Phys. Chem. C* **2014**, *118*, 13099.
[90] C. Chen, D.-F. Lu, R. Gao, Z.-M. Qi, *Opt. Commun.* **2016**, *367*, 86.
[91] T. Xu, L. Huang, C. Yin, Y. Jin, J. Fang, M. Huang, *Appl. Phys. Lett.* **2014**, *105*, 163703.

[92] Y. Wang, H. Li, Z. Cao, T. Yu, Q. Shen, Y. He, *Appl. Phys. Lett.* **2008**, *92*, 061117.
[93] C. Yin, Y. Lu, T. Xu, D. Z. Wei, Y. L. Jin, J. H. Fang, C. N. Wang, M. Z. Huang, *J. Raman Spectrosc.* **2016**, *47*, 560.
[94] T. Xu, Y. Lu, J. Li, C. Yin, Y. Jin, M. Wang, J. Fang, C. Wang, Y. Ge, *Appl. Optim.* **2017**, *56*, 115.
[95] Y. Wang, M. Huang, K. Wang, X. Liu, Y. Zou, B. Song, J. Chen, *J. Lightwave Technol.* **2016**, *34*, 3616.
[96] G. Baffou, *ACS Nano* **2021**, *15*, 5785.
[97] J. A. Jackman, N. J. Cho, *Langmuir* **2020**, *36*, 1387.
[98] H.-L. Wang, E.-M. You, R. Panneerselvam, S.-Y. Ding, Z.-Q. Tian, *Light Sci. Appl.* **2021**, *10*, 161.

How to cite this article: J. Zhao, X. Cao, W. Xu, S. Xu, *J Raman Spectrosc* **2024**, *55*(3), 355. https://doi.org/10.1002/jrs.6628